

SENSOR AND SIMULATION NOTES

NOTE 295

30 OCTOBER 1986

OPTIMIZATION OF THE ASYMPTOTIC
CONICAL DIPOLE EMP SENSORS

G.D. Sower

EG&G WASC, Inc.
Albuquerque, NM 87119

PL/PA 5/19/97

ABSTRACT

The Asymptotic Conical Dipole (ACD) D-dot sensors have been developed using the technique of an equivalent charge distribution. In this note we describe a more complicated equivalent charge distribution than has been hitherto used. This distribution results in a new ACD shape which is better than the old shape in that it is more asymptotic to the matched impedance cone at the sensor apex and hence exhibits an improved pulse fidelity response. The inherent accuracy of the produced sensors is also improved because extensive and accurate testing has resulted in a determination of the enhancement due to finite ground plate and sensor element support dimensions.

Approved for public release; distribution unlimited.

PL 96-1252

I. INTRODUCTION

A technique for the design of electric dipole antennas and sensors utilizing what is known as the equivalent-charge method has been developed in Reference 1. The technique consists of defining a hypothetical static charge distribution with total charge being equal to zero. We call this the equivalent-charge distribution. This distribution is usually defined such that it is rotationally symmetric about a particular axis (z-axis) with opposite charges reflected about the apex on the symmetry plane (x-y plane). The next step is to calculate the potential distribution due to this equivalent-charge distribution. Consider two of the equipotential surfaces thus generated of equal and opposite potential, which define two separate closed volumes, one around each of the equivalent charge distributions on each side of the symmetry plane. We may then make both of these surfaces into perfect conductors with the appropriate total surface charge such that the potential on the surfaces is the same as the equipotential values so that the potential distribution external to the surfaces remains unchanged. We have now defined an antenna geometry consisting of two equal symmetrical surfaces for which the potential distribution is known. The total antenna charge and the antenna dipole moment can be found as integrals over the equivalent-charge distribution. The antenna capacitance and mean charge separation are thus known, which also gives us the antenna sensitivity, expressed as an equivalent area.

Because we have postulated symmetry in the equivalent-charge distribution about the symmetry plane, the potential on this plane is exactly zero. We can therefore also make this a conducting surface of zero potential and obtain an antenna above a ground plane.

Any practical antenna must have some method for the introduction or pickoff of electrical signals. The two conducting surfaces described above must therefore approach each other at a common point. This point will necessarily be a discontinuity in the potential distribution. By symmetry, it will also lie on the zero potential plane and on the rotational axis. It is therefore convenient to define it as the origin of our coordinate system. In particular, we would like the shape of the surfaces to be asymptotic at the origin to some particular geometry which has a well-defined transmission line impedance. Such a geometry is the infinite biconical antenna.^{1,2,3} For an included conical half-angle of θ_0 we can define a variable θ_0 , which has possible values ranging from 0 to 1, as

$$\theta_0 = \tan\left(\frac{\theta_0}{2}\right) \quad (1)$$

for which the biconical surface potential is

$$\phi_s = \frac{\lambda_0}{4\pi\epsilon_0} \ln(\theta_0^{-2}) \quad (2)$$

This can be related to the biconical antenna characteristic impedance Z_c by

$$Z_c = \frac{Z_0}{\pi} \ln(\theta_0^{-1}) \quad (3)$$

where $Z_0 = \sqrt{\mu_0/\epsilon_0}$ is the free space wave impedance. This may also be written in terms of the geometric factor of a transmission line impedance

$$f_g = \frac{Z_c}{Z_0} \quad (4)$$

as

$$f_g = \frac{\ln(\theta_0^{-1})}{\pi} \quad (5)$$

II. FIRST GENERATION ACD SENSORS

The first generation of ACD sensors were constructed using the particular equivalent-charge distribution discussed in Reference 1. This consists of an equivalent line charge $\lambda(z)$ on the z-axis given by

$$\lambda(z) = \begin{cases} \lambda_0 & \text{for } 0 < z \leq z_0 \\ -\lambda_0 & \text{for } 0 > z \geq -z_0 \\ 0 & \text{for } z=0 \\ 0 & \text{for } |z| > z_0 \end{cases} \quad (6)$$

where $z_0 > 0$ and $\lambda_0 > 0$ is the uniform charge per unit length. The potential distribution from this equivalent charge is given, in cylindrical coordinates (r, ψ, z) (r as used here is the cylindrical radius), by

$$\phi = \frac{\lambda_0}{4\pi\epsilon_0} \ln \left\{ \frac{[z + \sqrt{z^2 + r^2}]^2}{[z+z_0 + \sqrt{(z+z_0)^2 + r^2}][z-z_0 + \sqrt{(z-z_0)^2 + r^2}]} \right\} \quad (7)$$

where ϕ is the potential at the point (r,z) . Notice that this potential distribution is rotationally symmetric (no ψ dependence).

We can now equate this potential with that for the infinite bicone, ϕ_s , which forces the resulting equipotential shape to be asymptotic to the bicone at the origin. The shape of the antenna sensing element is then given by

$$\theta_0^{-2} = \frac{[z + \sqrt{z^2 + r^2}]^2}{[z+z_0 + \sqrt{(z+z_0)^2 + r^2}][z-z_0 + \sqrt{(z-z_0)^2 + r^2}]} \quad (8)$$

where θ_0 is a constant determined by the desired asymptotic impedance given by (3). For each value of z between zero and the antenna height, h , there exists a unique value for the element radius r . The antenna height is determined by setting $r=0$ at $z=h$, which gives

$$h = \frac{z_0}{\sqrt{1 - \theta_0^2}} \quad (9)$$

Other sensor parameters may be readily calculated in terms of the antenna geometry. The charge on the positive surface is

$$Q_a = \int_0^{z_0} \lambda_0 dz = \lambda_0 z_0 \quad (10)$$

The dipole moment is given by

$$\vec{P} = 2\vec{e}_z \int_0^{z_0} \lambda_0 z dz = \lambda_0 z_0^2 \vec{e}_z \quad (11)$$

where \vec{e}_z is the vertical unit vector.

The antenna voltage is

$$V_a = \phi_s - (-\phi_s) = 2\phi_s \quad (12)$$

The capacitance between the two surfaces is thus

$$C_a = \frac{\lambda_o z_o}{2\phi_s} = \frac{\epsilon_o \pi z_o}{\ln(\theta_o^{-1})} \quad (13)$$

For one surface and a ground plane, the capacitance is

$$C_s = \frac{\lambda_o z_o}{\phi_s} = \frac{2\epsilon_o \pi z_o}{\ln(\theta_o^{-1})} \quad (14)$$

The mean charge separation distance is

$$\vec{h}_a = \vec{e}_z \frac{2}{Q_a} \int_0^{z_o} z \lambda_o dz = z_o \vec{e}_z \quad (15)$$

or in terms of the magnitude

$$h_a = z_o \quad (16)$$

The antenna equivalent area is obtained from

$$A_{eq} = \frac{C_a}{\epsilon_o} h_a \quad (17)$$

which gives

$$A_{eq} = \frac{\pi z_o^2}{\ln(\theta_o^{-1})} = \frac{z_o^2}{f_g} \quad (18)$$

We can thus choose a desired antenna sensitivity and impedance (the impedance for a monopole over a ground plane is half that of the corresponding dipole) and calculate the charge length z_o from

$$z_0 = \sqrt{A_{eq} f_g} \quad (19)$$

The element shape is then generated from (8) by choosing a value for z and determining the correct value for r by successive iterations. The calculations and element shapes for this equivalent-charge distribution are given in Reference 1 as a function of θ_0 . A family of ACD sensors based on these results has been manufactured in both dipole (free space) and monopole (ground plane) versions^{5,6,7,8,9,10,11} with sensitivities ranging from 1.00 square meter down to $1.00 \times 10^{-4} \text{ m}^2$. The characteristic impedance used is 50 ohms for a monopole, 100 ohms for a dipole.

Figure 1 shows one of the production sensors of the monopole version, the ACD-6A(A). The pulse response of this sensor has been tested in a conical simulator with a total measurement system rise time of 0.2 nanoseconds (Appendix A). Figure 2 shows this pulse response with the lower trace the actual sensor derivative output and the upper trace the time integral of the lower to show the sensor response to the step input electric field.

The ACD-6A(A) shows a rise time of 0.94 ns as measured between the 10 percent and 90 percent points of the final (settled) pulse height. It also exhibits a 10 percent overshoot with an associated underdamped ringing. From the standpoint of pulse fidelity, this is not an optimum pulse response - the overshoot and ringing are too large.

The pulse response of the ACD-6A(A) may be approximated to first order by the simple equivalent circuit shown in Figure 3. The capacitance and inductance are properties of the sensing element shape. Figure 3 also shows how closely this equivalent circuit describes the sensor response.

Figure 4 shows the ACD-6A(A) frequency response as calculated from the equivalent circuit model. Notice the peak in the spectrum which corresponds to the ring frequency of the damped oscillation of the pulse response. The transfer function is given in the frequency domain by

$$\frac{V_R(s)}{I(s)} = \frac{R}{s^2 LC + sRC + 1} \quad (20)$$

In the time domain this has three distinct solutions depending upon whether the oscillation is underdamped, critically damped, or overdamped:

$$\frac{V_R(t)}{I(t)} = R \begin{cases} \left[1 - \frac{\omega_0}{\omega} e^{-at} \sin(\omega t + \psi) \right] , & \omega_0^2 > a^2 \\ \left[1 - e^{-at} (1 + at) \right] , & \omega_0^2 = a^2 \\ \left[1 - \frac{\omega_0^2}{n-m} \left(\frac{1}{m} e^{-mt} - \frac{1}{n} e^{-nt} \right) \right] , & \omega_0^2 < a^2 \end{cases} \quad (21)$$

where

$$\omega_0^2 = \frac{1}{LC} , \quad a = \frac{R}{2L} , \quad \omega^2 = \omega_0^2 - a^2 , \quad \tan \psi = \omega/a ,$$

and

$$n, m = a \pm \sqrt{a^2 - \omega_0^2}$$

are the roots of $s^2 + 2as + \omega_0^2 = 0$.

For the special case of $L = 0$, this reduces to

$$\frac{V_R(t)}{I(t)} = R \left(1 - e^{-t/RC} \right) \quad (22)$$

When the sensor driving function, $I(t) = \vec{A}_{eq} \cdot \dot{\vec{D}}$, is a step function, the above equations give the sensor output response. When the incident field \vec{D} is a step function, $I(t)$ is the impulse function and the above equations must be differentiated with respect to time to give the sensor output response.

Desired Improvements

The first generation of ACD sensors possess good pulse and frequency response characteristics. However, these characteristics are not optimized in

the sense that the fidelity of the pulse response could be better in terms of less overshoot and ringing and the frequency response transfer function could be flatter at the higher frequencies.

In terms of the equivalent circuit parameters, the optimum frequency response is obtained when $2L = R^2C$. This is known as the "maximally flat" response which is shown in Figure 5. This occurs when L is twice that value which gives a critically damped response, also shown. Figure 5 also includes the ACD-6A(A) response and the response for the case $L = 0$. For a given value of resistance and capacitance, the flattest transfer function and the highest bandwidth (-3 dB point) occur for the maximally flat case.

This is also the case which gives about the best pulse fidelity as can be seen from Figure 6. It gives the fastest rise time with a slight overshoot (4.3%) which is then rapidly damped out without ringing.

The ACD sensors may thus be improved by decreasing the inductance of the sensing element to that required to give the maximally flat response. This should be accomplished with a minimum increase in the element capacitance. Specifically, the sensing element shape should be made "flatter" in the region near to the biconical apex, that is, to be made "more asymptotic" to the bicone.

A second desired improvement in the ACD sensor is in a more accurate determination of the enhancement factors resulting from those parts of the sensor other than the sensing element. In particular, the finite thickness of the ground plate and the dielectric support for the sensing element both tend to enhance the electric field as seen by the sensor. This effect results in a larger sensor output than would occur without the ground plate or support. In the past we have only been able to make an estimate of the worst-case enhancements. For the ground plate enhancement, a reasonable upper bound has been determined^{1,2} as

$$\Delta E \leq \frac{\pi}{2} \frac{h}{a} \quad (23)$$

where h is the plate thickness and a the plate radius. The lower bound has been taken as zero enhancement. The enhancement has then been estimated as the average of these upper and lower bounds with the corresponding error in the estimate:

$$\Delta E = \frac{\pi h}{4 a} \pm \frac{\pi h}{4 a} \quad (24)$$

Thus, if the plate radius is only, say, twenty times as much as its height, a sensitivity uncertainty of about four percent results. Note also that the above estimate does not include any effect of the sensing element dimensions with respect to the plate dimensions.

The dielectric support structure used to physically support the ACD sensing element also creates an enhancement in \vec{D} as seen by the sensor. Two types of supports have been used: a hemispherical dome for the smaller sensors and a cylinder for the larger ones. Neither of these geometries lends itself to an analytical solution for the ACD enhancement as a function of dielectric thickness and dielectric constant. While the dome is located over the entire sensing element where its effect is fully manifested, the cylindrical support is located below the sensing element where the fields are minimum and so its effect is minimized. Further, its surface is nearly normal to the electric fields in this region, so the distortion of these fields is also minimized. The cylindrical support is thus to be preferred to the dome.

Any optimization of the ACD sensors should include a better determination of these enhancement factors. A computer model study of the rotationally symmetric static potential distribution is possible and should result in an accurate determination. It is also possible to make an experimental determination by comparing sensor outputs with various ground plate geometries and dielectric cylinder thicknesses. Accuracies on the order of one percent are obtainable with this method.

Once the enhancement factors for a certain ACD configuration are known, the sensing element size is reduced by that amount necessary to maintain the desired sensitivity.

III. MODIFICATION OF THE EQUIVALENT-CHARGE DISTRIBUTION

Consider now a modification to the equivalent-charge distribution discussed in Section II and Reference 1 by the addition of a point charge of magnitude $\pm Q_0$ at the ends of the line charges at $\pm z_0$. We will proceed to show that this equivalent-charge distribution, for a particular value of Q_0 , gives an antenna shape which has a very nearly ideal pulse and bandwidth response and is asymptotic to the biconical transmission line for a distance much farther from the apex than previous shapes.

This equivalent-charge distribution is given by:

$$\lambda(z) = \begin{cases} Q_0, & z=z_0 \\ -Q_0, & z=-z_0 \\ \lambda_0, & 0 < z < z_0 \\ -\lambda_0, & 0 > z > -z_0 \\ 0, & z=0, z > z_0 \end{cases} \quad (25)$$

$$Q_0 > 0, \lambda_0 > 0, z_0 > 0$$

The potential distribution of this charge distribution is the superposition of the potentials from the point charges and the distributed charges. The potential function generated by the line charges is already given by equation (7). The potential at a point (z,r) due to the two point charges is given by

$$\phi_p = \frac{Q_0}{4\pi\epsilon_0} \left\{ \frac{1}{\sqrt{(z-z_0)^2 + r^2}} - \frac{1}{\sqrt{(z+z_0)^2 + r^2}} \right\} \quad (26)$$

Let us now relate the magnitude of the point charges to that of the line charges. The total charge on the positive line segment is $\lambda_0 z_0$. We define a dimensionless quantity α as the ratio of the point charge to the line charge, so that

$$Q_0 = \alpha \lambda_0 z_0 \quad (27)$$

Note that $\alpha = 0$ for the original ACD sensor shapes.

When we equate the total potential distribution to that for the infinite bicone, ϕ_s , the (z,r) coordinates for the antenna shape are now given in terms of θ_0 by

$$\ln(\theta_0^{-2}) = \ln \left\{ \frac{[z + \sqrt{z^2 + r^2}]^2}{[z+z_0 + \sqrt{(z+z_0)^2 + r^2}][z-z_0 + \sqrt{(z-z_0)^2 + r^2}]} \right\} \\ + \frac{\alpha z_0}{\sqrt{(z-z_0)^2 + r^2}} - \frac{\alpha z_0}{\sqrt{(z+z_0)^2 + r^2}} \quad (28)$$

The antenna element height is again determined by setting $r=0$ at $z=h$, which gives

$$\ln(\theta_0^{-2}) = \ln\left(\frac{h^2}{h^2 - z_0^2}\right) + \frac{2\alpha z_0^2}{h^2 - z_0^2} \quad (29)$$

For any given θ_0 , α , and h this equation must be solved for z_0 by iterative techniques. Figure 7 shows the values of z_0 , normalized to the antenna height h , as a function of θ_0 for various values of α .

Antenna shapes for various values of θ_0 are shown in Figures 8-16 for different values of α from 0 (original ACD) to 10. The point charge for small values of α manifest itself first as small changes in the shape of the equipotentials near the top of the sensor for small values of θ_0 (Figures 9 and 10). For values of α near unity (Figure 12) the effect of the point charge becomes more visible, expanding the equipotential contours around it appreciably. For large values of α (Figures 15 and 16), the fields from the point charge dominate the equipotential surfaces, except for the region very close to the line charge.

For the limiting case of $\theta_0 = 1$, the length of the line charge z_0 becomes zero and the equivalent charge distribution becomes that of a point dipole. The extra charge placed at z_0 by the point charge only serves to change the magnitude of this dipole, so the potential distribution does not depend upon the value of α . The dipole potential at a point (z,r) is given by

$$\phi_d = \frac{pz}{[z^2 + r^2]^{3/2}} \quad (30)$$

At the normalized height $z=h$, r is zero, so

$$\phi_d = \frac{p}{h^2} \quad (31)$$

The shape of an antenna for this particular potential is thus given by

$$\frac{z}{h} = \left[\left(\frac{z}{h}\right)^2 + \left(\frac{r}{h}\right)^2 \right]^{3/2} \quad (32)$$

which can be solved for r in terms of z :

$$\frac{r}{h} = \left[\left(\frac{z}{h} \right)^{2/3} - \left(\frac{z}{r} \right)^2 \right]^{1/2} \quad (33)$$

This contour is shown on all of the graphs for $\theta_0 = 1$. The maximum radius occurs when

$$\frac{dr}{dz} = 0 \quad (34)$$

This happens at $z/h = (1/3)^{3/5} = .438691$, for which $r/h = .620403$.

The shapes of the equipotential contours can be seen more easily in Figures 17, 18, and 19 for values of α of 0, 1, and 2, respectively. Each of these figures has an equivalent-charge height of unity and shows the contours for various values of θ_0 .

Of special interest in the construction of ACD sensors are the antenna contours for certain characteristic impedances common in electrical circuits. Figures 20, 21, and 22 show contours for various values of α for bicone antenna characteristic impedances of 50, 100, and 200 ohms, respectively. Of particular interest is Figure 21 which shows the contours for 100-ohm differential or 50-ohm single-ended impedance. This is the impedance for which ACD sensors have been built, and the $\alpha=0$ curve shows the old shape.

Also included in Figures 20-22 is the bicone angle for each characteristic impedance, shown as the thin, straight line. Notice that for each characteristic impedance, the value $\alpha=1$ appears to give the best asymptotic fit of the ACD contour to the bicone. This will be discussed in detail in the next section.

The other sensor parameters of interest can now be calculated in terms of the antenna geometry. The charge on the positive surface is

$$Q_a = \lambda_0 z_0 + \alpha \lambda_0 z_0 = (1+\alpha) \lambda_0 z_0 \quad (35)$$

The dipole moment is

$$\vec{p} = \vec{e}_z \lambda_0 z_0^2 + \vec{e}_z 2\alpha \lambda_0 z_0^2 = (1+2\alpha) \lambda_0 z_0^2 \vec{e}_z \quad (36)$$

The antenna voltage is

$$V_a = 2\phi_s \quad (37)$$

The capacitance between the two surfaces is

$$C_a = \frac{Q_a}{V_a} = \frac{(1+\alpha) \lambda_o z_o}{2\phi_s} = (1+\alpha) \frac{\epsilon_o \pi z_o}{\ln(\theta_o^{-1})} = \frac{\epsilon_o}{f_g} (1+\alpha) z_o \quad (38)$$

Figure 23 shows values of C_a , normalized to $\frac{C_a}{\epsilon_o h}$, as a function of θ_o for various values of α . The capacitance for one surface over a ground plane is

$$C_s = \frac{Q_a}{\phi_s} = (1+\alpha) \frac{2\epsilon_o \pi z_o}{\ln(\theta_o^{-1})} = \frac{2\epsilon_o}{f_g} (1+\alpha) z_o = 2C_a \quad (39)$$

The mean charge separation distance is

$$\vec{h}_a = \frac{\vec{p}}{Q_a} = \frac{1+2\alpha}{1+\alpha} z_o \vec{e}_z \quad (40)$$

or in terms of the magnitude

$$h_a = \frac{1+2\alpha}{1+\alpha} z_o \quad (41)$$

The antenna equivalent area is thus

$$A_{eq} = \frac{C_a}{\epsilon_o} h_a = (1+2\alpha) \frac{\pi z_o}{\ln(\theta_o^{-1})} = (1+2\alpha) \frac{z_o^2}{f_g} \quad (42)$$

Figures 24 and 25 show values of A_{eq} normalized to πh^2 , as a function of θ_o for various values of α . The capacitance can then be written in terms of the equivalent area

$$C_a = \frac{1+\alpha}{1+2\alpha} \frac{\epsilon_o A_{eq}}{z_o} \quad (43)$$

The equivalent charge height z_0 can be eliminated using 37 to give

$$C_a = \frac{1 + \alpha}{\sqrt{1 + 2\alpha}} \epsilon_0 \sqrt{\frac{A_{eq}}{f g}} \quad (44)$$

IV. OPTIMIZATION OF THE MAGNITUDE OF THE POINT CHARGE

We want the shape of the ACD sensing element to closely approximate the conical geometry for as far from the apex as possible. (An ideal ACD shape would perhaps be that of a cone with a spherical cap; an "ice cream cone".) An examination of Figures 8-22 shows that the geometry of the base of the element is highly dependent upon the point charge magnitude, represented by the dimensionless parameter α . We must therefore determine what value of α gives a shape which closely approximates that of a cone; that is, is "most asymptotic" to the biconical antenna.

We first need to determine what we mean by "most asymptotic". Obviously we want the radius of the shape, $r(z)$, to be as similar as possible to the radius of the cone, $z \tan \theta_0$. Thus, one definition of "most asymptotic" is to minimize the magnitude of the term

$$r(z) - z \tan(\theta_0) \quad (50)$$

for as large a value of z as possible. Certainly we can set this expression equal to zero at the apex and be very close to zero for small values of z .

Another definition arises from taking the derivative of (50) with respect to z to obtain the slope of the shape, and to then minimize the resulting expression:

$$r'(z) - \tan(\theta_0) = 0 \quad (51)$$

Again, we can set this identically equal to zero at the apex.

Higher order derivatives gives us further possibilities:

$$r''(z) = 0 \quad (52)$$

$$r'''(z) = 0, \text{ etc.} \quad (53)$$

The best definition of most asymptotic may therefore be the one which is to have as many derivatives as possible to be zero at the apex.

The shape of the ACD element is given by the cylindrical coordinates (z,r) where $r(z,\alpha, \theta_0)$ is the radius at height z for given values of α and θ_0 . The value of r is defined by the transcendental equation

$$\ln(\theta_0^{-2}) = F(r,z,\alpha) \quad (54)$$

which is a constant for any given value of θ_0 . There are several equivalent expressions which may be used to represent F . Near the origin F is best defined by

$$F = \ln \left\{ \left[\frac{z + \sqrt{z^2 + r^2}}{r} \right]^2 \left[\frac{z_0 - z + \sqrt{(z_0 - z)^2 + r^2}}{z_0 + z + \sqrt{(z_0 + z)^2 + r^2}} \right] \right\} \\ + \frac{\alpha z_0}{\sqrt{(z_0 - z)^2 + r^2}} - \frac{\alpha z_0}{\sqrt{(z_0 + z)^2 + r^2}} \quad (55)$$

We find the first derivative of the implicit function $r(z,\alpha)$ with respect to z at constant α by the partial differentiation of $F(r,z,\alpha)$:

$$\frac{dF}{dz} = \left. \frac{\partial F}{\partial z} \right|_{\alpha} + \left. \frac{\partial F}{\partial r} \right|_{\alpha} \frac{dr(z)}{dz} \Big|_{\alpha} \quad (56)$$

This expression must be identically zero because F is a constant. Therefore, for constant α ,

$$\frac{dr}{dz} = - \frac{\left(\frac{\partial F}{\partial z} \right)}{\left(\frac{\partial F}{\partial r} \right)} \quad (57)$$

Using logarithmic differentiation, we obtain from (55)

$$\frac{\partial F}{\partial z} = \frac{2}{\sqrt{z^2 + r^2}} - \frac{1}{\sqrt{(z_0 - z)^2 + r^2}} - \frac{1}{\sqrt{(z_0 + z)^2 + r^2}} \\ + \frac{\alpha z_0 (z_0 - z)}{[(z_0 - z)^2 + r^2]^{3/2}} + \frac{\alpha z_0 (z_0 + z)}{[(z_0 + z)^2 + r^2]^{3/2}} \quad (58)$$

$$\begin{aligned}
\frac{\partial F}{\partial r} = & - \frac{2z}{r\sqrt{z^2 + r^2}} + \frac{r}{\sqrt{(z_0 - z)^2 + r^2} [z_0 - z + \sqrt{(z_0 - z)^2 + r^2}]} \\
& - \frac{r}{\sqrt{(z_0 + z)^2 + r^2} [z_0 + z + \sqrt{(z_0 + z)^2 + r^2}]} \\
& - \frac{\alpha z_0 r}{[(z_0 - z)^2 + r^2]^{3/2}} + \frac{\alpha z_0 r}{[(z_0 + z)^2 + r^2]^{3/2}} \tag{59}
\end{aligned}$$

Near the apex we have $z \ll z_0$ and $r \ll z_0$ so we may expand (58) and (59) retaining only terms to the first order in $\frac{z}{z_0}$ and $\frac{r}{z_0}$:

$$\frac{\partial F}{\partial z} = \frac{2}{\sqrt{z^2 + r^2}} + \frac{2(\alpha-1)}{z_0} \tag{60}$$

$$\frac{\partial F}{\partial r} = - \frac{2z}{r\sqrt{z^2 + r^2}} \tag{61}$$

Therefore, using (57), (60), and (61) we obtain the value for the slope of the element near the apex:

$$r'(z) = \frac{dr}{dz} = \frac{r}{z} \left[1 + (\alpha-1) \frac{\sqrt{z^2 + r^2}}{z_0} \right] \tag{62}$$

This reduces to

$$r'(0) = \frac{r}{z} \tag{63}$$

at the apex, as expected. This value is independent of the value of α . Note that the slope near the apex as given by (62) reduces to the value at the apex if $\alpha=1$. We therefore expect that this value of α is the optimum value. This is confirmed by calculation of the rate-of-change of the slope near the apex.

Near the apex we may find the value of the second derivative of the shape of the ACD curve, $r''(z)$, by taking the total derivative of the implicit function $r'(z)$ given by (62) with respect to z . Thus

$$r''(z) = \frac{d}{dz} (r'(z)) = \frac{d}{dz} \left[\frac{r}{z} + \frac{(\alpha-1)}{z_0} \frac{r}{z} \sqrt{z^2 + r^2} + o\left(\frac{z^2}{z_0^2}, \frac{r^2}{z_0^2}\right) \right] \quad (64)$$

from which we obtain the expression near the apex.

$$r''(z) = \frac{r}{z} \left[\frac{2(\alpha-1)}{z_0} \frac{\sqrt{z^2 + r^2}}{z} + \frac{(\alpha-1)^2}{z^2} \frac{z^2 + 2r^2}{z} + o\left(\frac{z}{z_0}, \frac{r}{z_0}\right) \right] \quad (65)$$

At the apex this reduces to

$$r''(0) = \frac{2(\alpha-1)}{z_0} \frac{r}{z} \sqrt{1 + \left(\frac{r}{z}\right)^2} \quad (66)$$

where the value of r/z is the slope at the origin given by (63). This expression is zero only if α is identically equal to unity, which must therefore be its optimum value. This requirement is true for all values of θ_0 . Numerical calculations agree with this value to the limit of round-off errors.

The solution for $r''(0) = 0$, which determines the value of α to be unity, yields the antenna shape for which is the most asymptotic to the bicone for the longest distance from the origin, as observed in Figures 20, 21, and 22. For some values of θ_0 , however, it does not yield what may be considered the best antenna shape. Figure 12 shows that the shape determined by $\alpha=1$ becomes concave for small values of θ_0 . That is, the value for $r''(z)$ becomes positive and $r(z)$ becomes greater than $z \tan \theta_0$ - most of the antenna is larger in radius than the bicone.

The exact value of θ_0 below which this effect occurs appears to be about $\theta_0 = .3564$, which corresponds to $\tan \theta_0 = \sqrt{2/3}$. Proof that this result is exact remains elusive.

V. PERFORMANCE OF NEW ACD SENSORS

A new generation of ACD sensors has been developed based upon the shapes with $\alpha=1$. The ACD-6B(A) is shown in Figure 26.

It is interesting to compare the sensor parameters for the new shape to those of the prior ACD sensing element for the case where the two elements

have the same equivalent area. For both elements, the values of λ_o and ϕ_s are the same. Figure 27 shows the two shapes. The comparisons give, for $\alpha=1$:

$$A_{eq}(new) = A_{eq}(old)$$

$$z_o(new) = \frac{1}{\sqrt{3}} z_o(old)$$

$$h_a(new) = \frac{\sqrt{3}}{2} h_a(old)$$

$$p(new) = p(old)$$

$$C(new) = \frac{2}{\sqrt{3}} C(old) \quad (67)$$

The sensor capacitance has thus been increased by 15 percent. The inductance of the sensing element has at the same time been decreased due to the shorter and wider shape of the new sensing element, however, no convenient analytical expression is available for making this calculation.

This sensor was tested for pulse response in the Conical Elliptical Simulator as discussed in Appendix A. A reproduction of the actual data trace is shown in Figure 28. The bottom trace is the actual sensor output, showing the sensor derivative response to the step-function incident field. The top trace is the integrated response.

This response is noticeably better than that of the ACD-6A(A). This can be better seen in Figure 29, where the two responses are shown together. The new shape gives less than half the overshoot and ringing of the old shape. The 10- to 90-percent rise time is slightly slower for the new shape, due to the increased capacitance of the element, 1.02 ns as compared to 0.94 ns for the ACD-6A(A). The overall gain in pulse fidelity, however, is significant.

The new ACD can be modeled by the equivalent circuit shown in Figure 30, which gives the shown pulse response. The capacitance has increased by 13 percent, very close to the 15 percent predicted. The inductance has decreased by 29 percent, twice as much as the increase in capacitance.

The calculated bandwidth of this new ACD-6 sensor is shown in Figure 31, along with that of the ACD-6A(A). Both are obtained from their equivalent circuits, and are represented by

$$\frac{V_{out}}{R \vec{A}_{eq} \cdot \vec{D}} = \frac{1}{(1 - \omega^2 LC) + j\omega RC} \quad (68)$$

in the complex frequency domain. Only the amplitude variation with frequency ω is shown here. The new ACD is very close to a maximally flat response. In fact, for the values of R and C given in the equivalent circuit model, the maximally flat response results in a value for the inductance of 16.9 nH. The -3 dB point for the new ACD-6 is slightly less (7.5 percent) than that for the ACD-6A(A). However, its response is better up to about 200 MHz.

Time Domain Reflectometer (TDR) responses of both the old and new ACD-6 sensors are shown in Figure 32. This is a measure of the characteristic impedance of the sensor at various points on its surface as seen by an input step waveform driven onto its apex (output connector). The new shape shows the 50 ohm characteristic impedance almost all the distance up the sensor to the point where the dielectric support is fastened. The ACD-6A(A) shows a significantly larger deviation from the 50 ohm input impedance.

We may define a figure of merit Λ for the ACD sensors^{5, 12} as

$$\Lambda = \sqrt{\frac{R}{z_0}} \frac{A_{eq}}{\ell_c^2} \quad (69)$$

where R is the output load resistance, $z_0 = \sqrt{\mu_0/\epsilon_0}$ is the wave impedance of free space, and ℓ_c is a characteristic length related to the sensor rise time or bandwidth as

$$\ell_c = ct_c \quad \text{or} \quad \ell_c = \frac{c}{\omega_c} \quad (70)$$

In common usage, t_c is defined as the 10- to 90-percent rise time and $\omega_c = 2\pi f_c$ where f_c is the upper 3-dB point of the frequency response.

We actually wish to utilize a figure of merit which includes both the sensor rise time and bandwidth. Let us therefore use

$$\ell_c^2 = \frac{c^2 t_c}{\omega_c} \quad (71)$$

as our defining relationship. For the ACD-6A(A) sensor we have a rise time of 0.94 ns and a bandwidth of 360 MHz which gives a value for Λ_{avg} of 0.974. The new ACD-6 prototype has a rise time of 1.02 ns and a bandwidth of 335 MHz for a Λ_{avg} of 0.835. This lower value of Λ_{avg} for the new ACD-6 reflects the slightly lower bandwidth and slower rise time due to the increase in sensor capacitance.

VI. PULSE FIDELITY DEFINITION

The figure of merit as defined above includes no mention of the pulse fidelity, or how well the sensor output approximates the shape of the incident field. Let us therefore define a pulse fidelity factor, η , which is a measure of how well the sensor reproduces the incident field.

The figure of merit Λ_{avg} includes a measure of the 10- to 90-percent rise time of the sensor. Let us therefore define an "ideal" sensor response to a step input as a straight line ramp joining the 10 percent and 90 percent points of the sensor output as shown in Figure 33. Before the intersection of this line with the 0 percent point and after the intersection with the 100 percent point, the curve will be a flat line with no slope. By defining the ideal waveform in this manner we allow for the finite sensor rise time and say that the incident step field should be slewed over into a ramp by the rise time.

Now, how can we estimate how well the actual sensor response follows this ramp? One way would be to find the total area difference between the two curves in Figure 33 (normalized to the step height and rise time). We would want η to become unity as this area goes to zero, and η to go to zero as this area becomes large. This is an aesthetic way of defining η , but unfortunately a very difficult way of calculating it. Another method could utilize the principle of least squares whereby the integral (or sum if digitized data traces are employed) of the square of the instantaneous deviations between the two lines is calculated. Again, as this value goes to zero, η goes to unity. This is also a difficult calculation to perform.

A much easier way to estimate η is to simply measure the largest deviation between the two curves. Let ζ be this deviation, normalized to the pulse height. ζ should never be greater than unity: at unity the sensor response is totally undamped and rings forever as $1 + \cos\omega t$. In this case η

should be zero. A ζ of 0.5 is a very large overshoot, so we would like the corresponding value of η to be small. Therefore η should be a nonlinear function of ζ , perhaps like

$$\eta = (1 - \sqrt{\zeta})^2 \quad (72)$$

or

$$\eta = (1 - \zeta)^4 \quad (73)$$

More work needs to be done on defining η , but we can use the estimation given by (73) to evaluate the ACD sensors. For the ACD-6A(A) we get a value of $\eta = 0.627$ and for the new ACD-6 we get $\eta = 0.839$. This gives us a numerical estimate of how much better pulse fidelity the new ACD shape gives.

If we now combine the figure of merit and the pulse fidelity used above, we obtain an overall measure of the sensor performance. For the ACD-6A(A) this is $\Lambda\eta = 0.611$. For the new ACD-6 it is $\Lambda\eta = 0.700$. This indicates that the new shape is somewhat better than the old ACD shape.

VII. ENHANCEMENT FACTOR DETERMINATION

A prototype ACD-6 sensor was made with a minimum thickness dielectric support cylinder and with a ground plate which mounts flush with the test simulator ground plane so that the enhancement factors were essentially zero. Conducting spacers of varying thickness and radii were made to go under the sensor, as were dielectric sleeves to go around the support cylinder. In this manner the enhancement factors were measured by a comparison to the sensor response without enhancement of one percent.

The experimental setup used was that described in Appendix A. The rms error on any measurement was about one percent, so this is the accuracy of the enhancement factor determination.

A dielectric sleeve of thickness 0.125 inch was used to measure the enhancement from the cylindrical support. The enhancement from this sleeve could not be measured as it was less than one percent. Thicker sleeves need to be used, but this has not yet been done. We do at least now have an upper bound on this enhancement of one percent.

Cylindrical plates of radius 7.00 and 14.00 inches and thickness increments of 0.25 inch were used to measure the ground plate enhancement

factor. A typical data record for one of these spacers is shown in Figure 34. Five sweeps of the sensor output, both with the spacer plate and without it, were recorded so as to give a measure of the system noise (one percent). The enhancement for this spacer is equal to the percentage difference between the means of the two runs. In this case, for a plate of 0.50 inch thickness and 7.00 inch radius, the enhancement was 8.2 percent (± 1 percent).

The enhancement is also a function of the size of the sensing element. This can be normalized out by basing the enhancement calculation on the ratio of the spacer plate dimensions to the height of the ACD sensing element. This height is 6.04 inches for the ACD-6 prototype. The normalized data are shown in Figure 35 as a function of the ratio of the plate thickness to sensor height for the two plate radii. A fit to these data gives an expression for the enhancement factor, E.F., expressed as a percentage as

$$E.F. = 72 \left(\frac{T}{H} \right) \left(\frac{R}{H} \right)^{-0.7} \text{ percent} \quad (74)$$

By using the above data for enhancement factors, we may now build ACD sensors which are accurate in their sensitivity to within one percent.

VIII. SUMMARY

A new equivalent charge distribution has been used to generate a new shape for the Asymptotic Conical Dipole sensors. The addition of a point charge to the end of the linear charge distribution, with a value exactly equal to the total charge of the linear charge yields a shape which maximizes the asymptoticness to a bicone. This new shape gives a more optimized pulse response and a flatter frequency response over the sensor bandwidth. The sensor enhancement factors, which previously had only been estimated from crude models, have now been determined to an accuracy of one percent. This allows for the production of more accurate sensors than in the past.

REFERENCES

1. C.E. Baum, "An Equivalent-Charge Method for Defining Geometries of Dipole Antennas", SSN 72, January 1969.
2. C.E. Baum, "A Circular Conical Antenna Simulator", SSN 36, March 1967.
3. C.E. Baum, "Design of a Pulse Radiating Dipole Antenna as Related to High-Frequency and Low-Frequency Limits", SSN 69, January 1969.
4. C.E. Baum, "Parameters for Some Electrically-Small Electromagnetic Sensors", SSN 38, March 1967.
5. C.E. Baum, E.L. Breen, J.C. Giles, J.P. O'Neill, and G.D. Sower, "Sensors for Electromagnetic Pulse Measurements Both Inside and Away from Nuclear Source Regions", IEEE Trans. on Antenna Propagation, January 1978; also IEEE Trans. Electromagnetic Compat. February 1978, also AFWL Sensor and Simulation Note 239, January 1978.
6. C.E. Baum, E.L. Breen, C.B. Moore, J.O. O'Neill, and G.D. Sower, "Electromagnetic Sensors for General Lightning Application", Proc. Lightning Tech. NASA Conf. Pub. 2128 and FAA-RD-80-30, April 1980, pp 85-118.
7. C.E. Baum, E.L. Breen, F.L. Pitts, G.D. Sower, and M.E. Thomas, "The Measurement of Lightning Environmental Parameters Related to Interaction with Electronic Systems," IEEE Trans. Electromagnetic Compat., May 1982.
8. V.V. Liepa and T.B.A. Senior, "Measured Characteristic of MGL and ACD Sensors", Sensor and Simulator Note 276, September 1982.
9. S.L. Olsen, "Asymptotic Conical Dipole D-Dot Sensor Development", AFWL-TR-75-263, January 1976 (also EG&G AL-1185, September 1975).
10. G.D. Sower, "Asymptotic Conical Dipole (ACD) Sensor Development", Nuclear EMP Meeting, June 1978.
11. G.D. Sower, "Asymptotic Conical Dipole ACD-6A(A) Sensor Development", EG&G AG-1456, August 1980.
12. C.E. Baum, "Some Further Consideration for the Circular Parallel Plate Dipole", SSN 86, June 1969.
13. C.E. Baum, "A Figure of Merit for Transit-Time-Limited Time-Derivative Electromagnetic Field Sensors", SSN 212, December 1975.

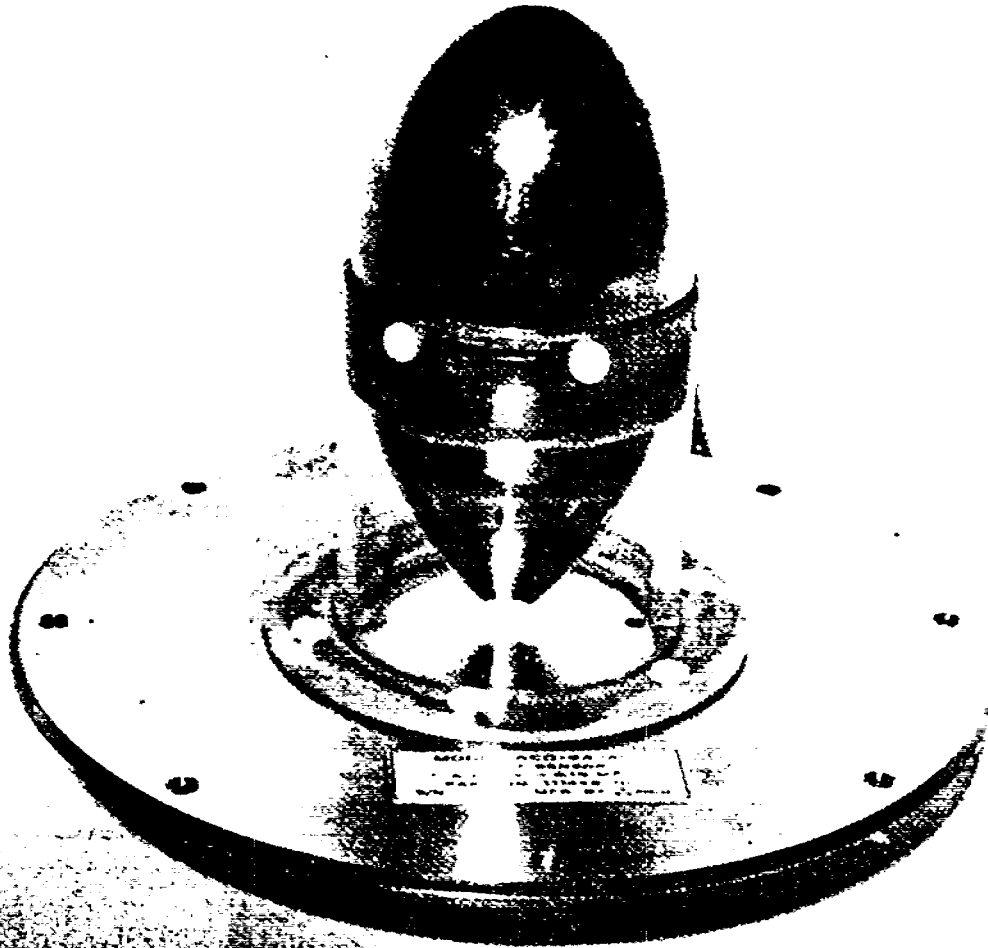


Figure 1. ACD-6A(A) Sensor

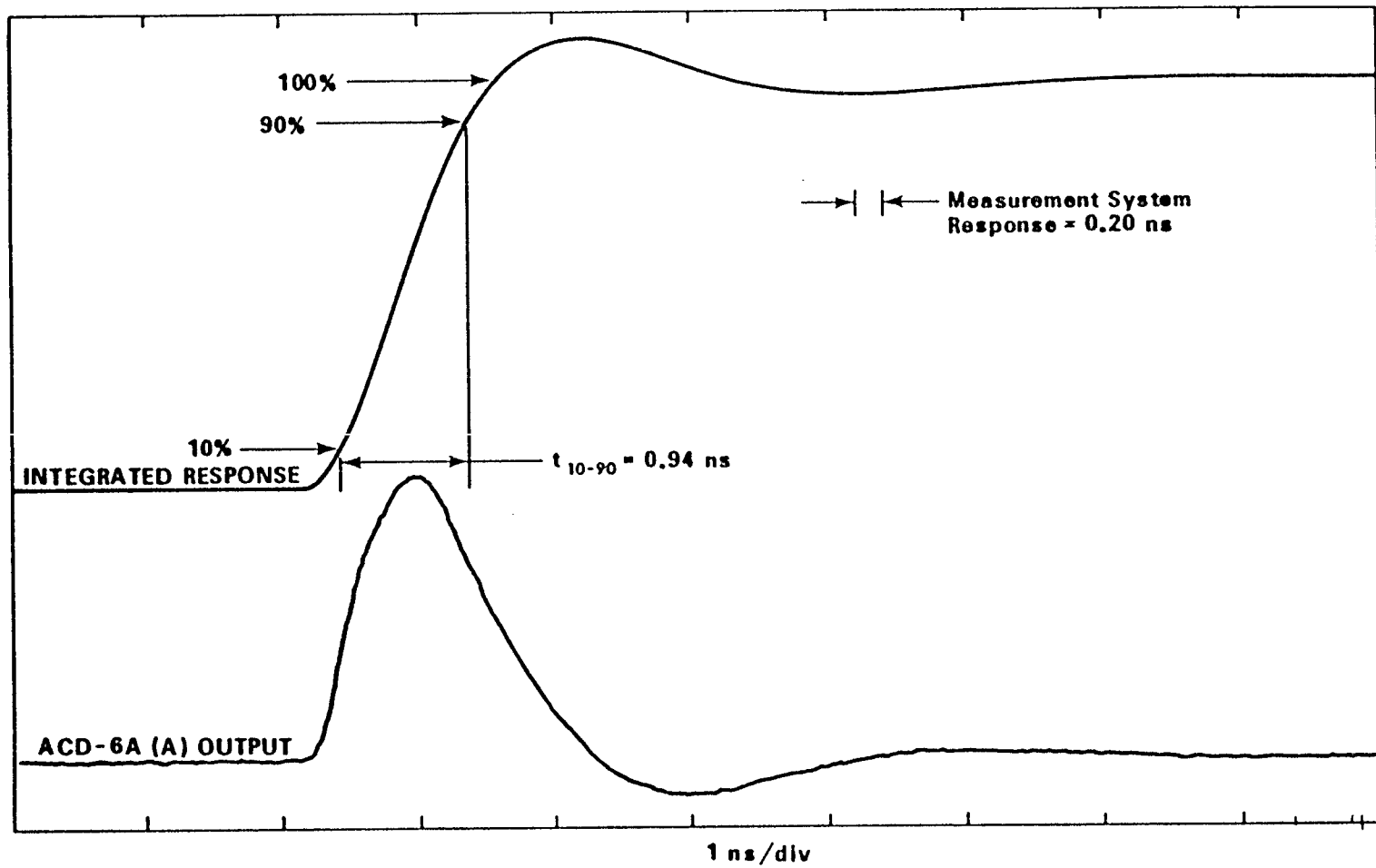
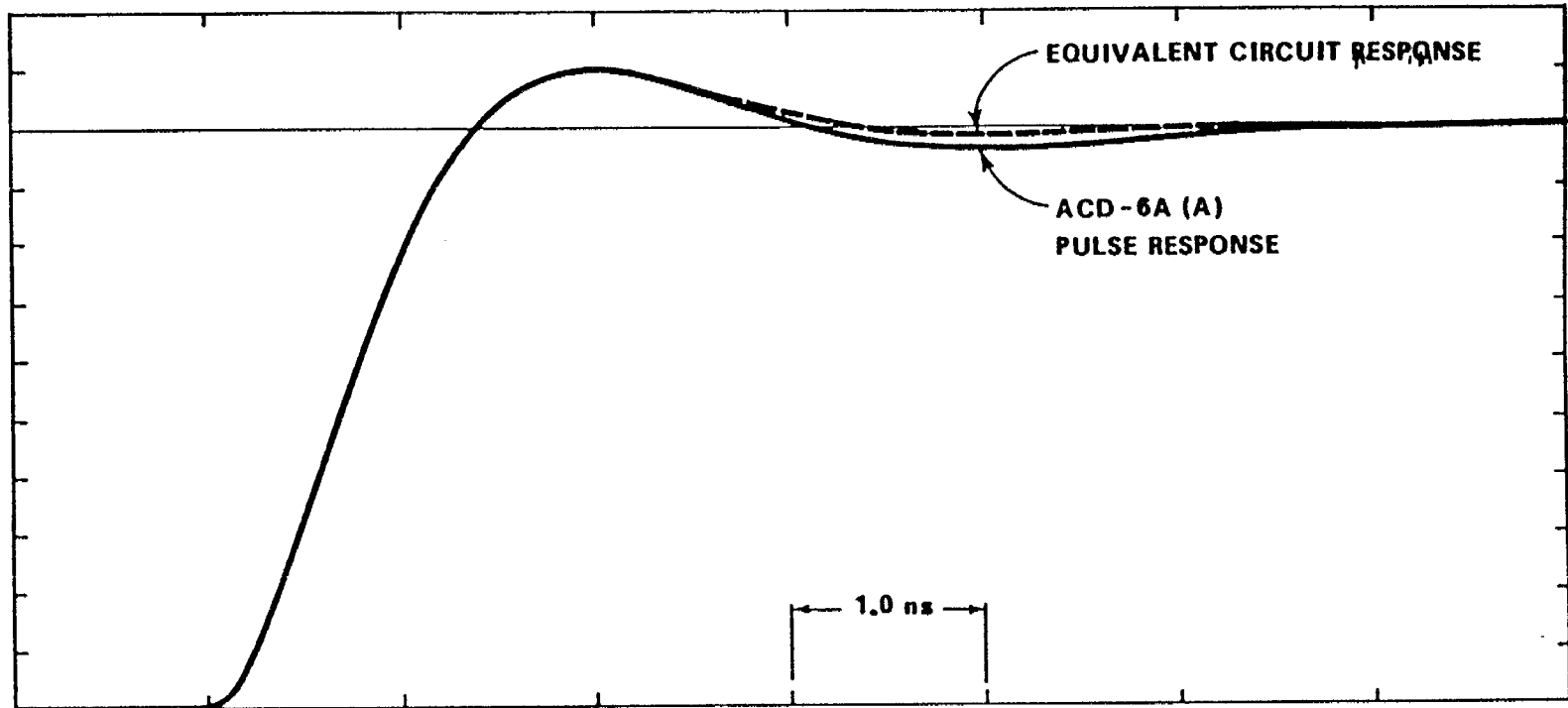
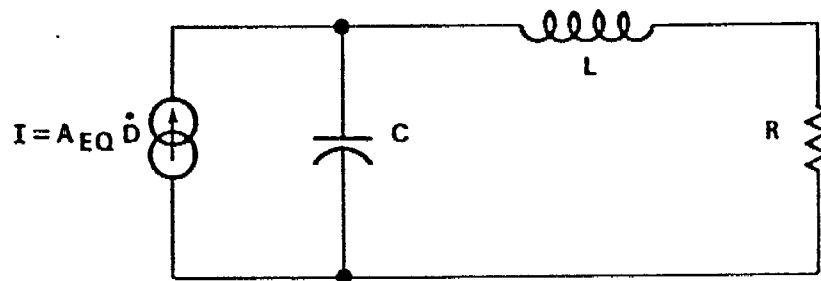


Figure 2. ACD-6A(A) Pulse Response



EQUIVALENT CIRCUIT OF ACD-6A (A) SENSOR



$C = \text{Element Capacitance} = 12\text{pF}$

$L = \text{Element Inductance} = 22\text{nH}$

$R = \text{Load Resistor} = 50\Omega$

Figure 3. ACD-6A(A) Equivalent Circuit and Pulse Response Comparison

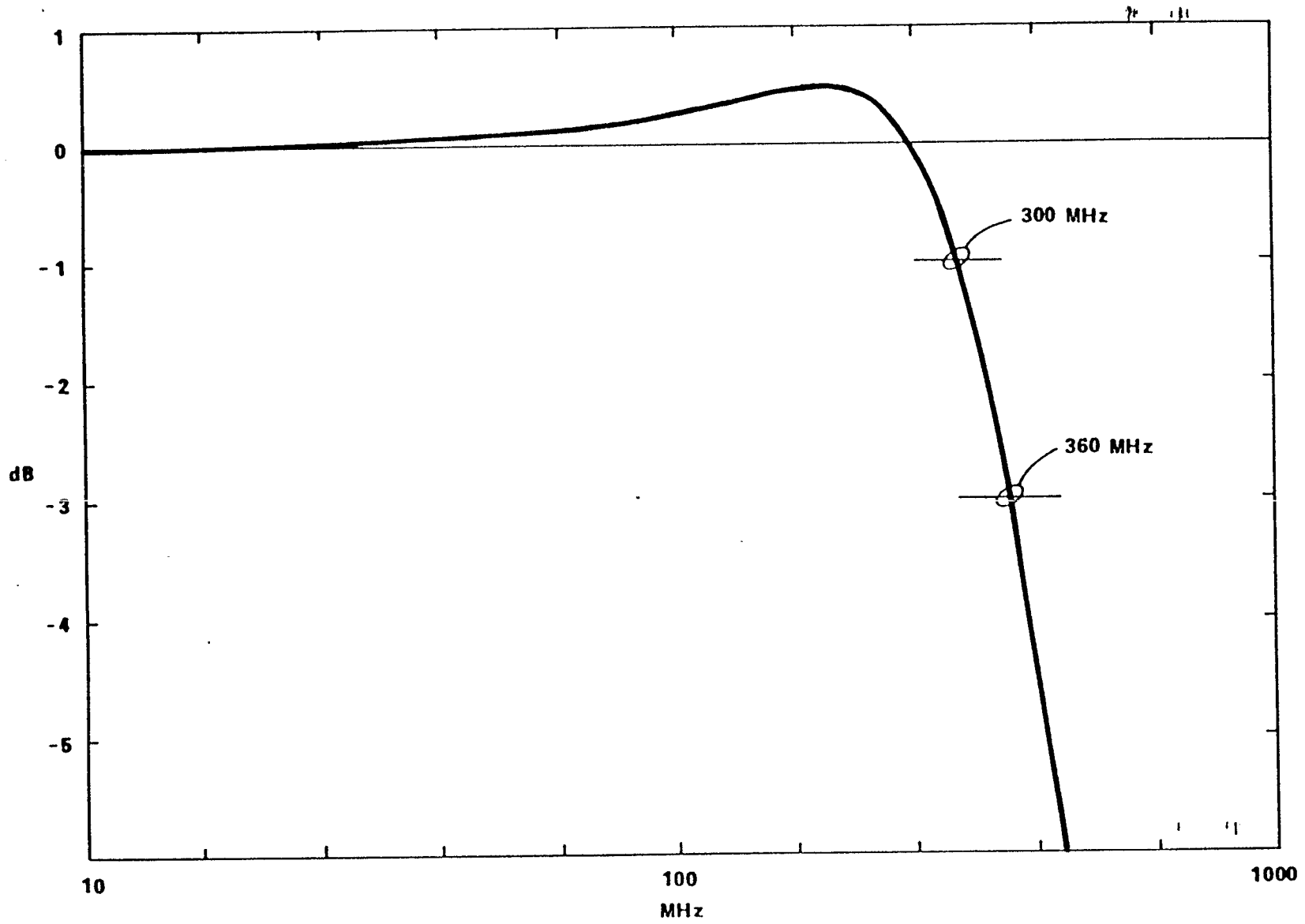


Figure 4. ACD-6A(A) Calculated Frequency Response

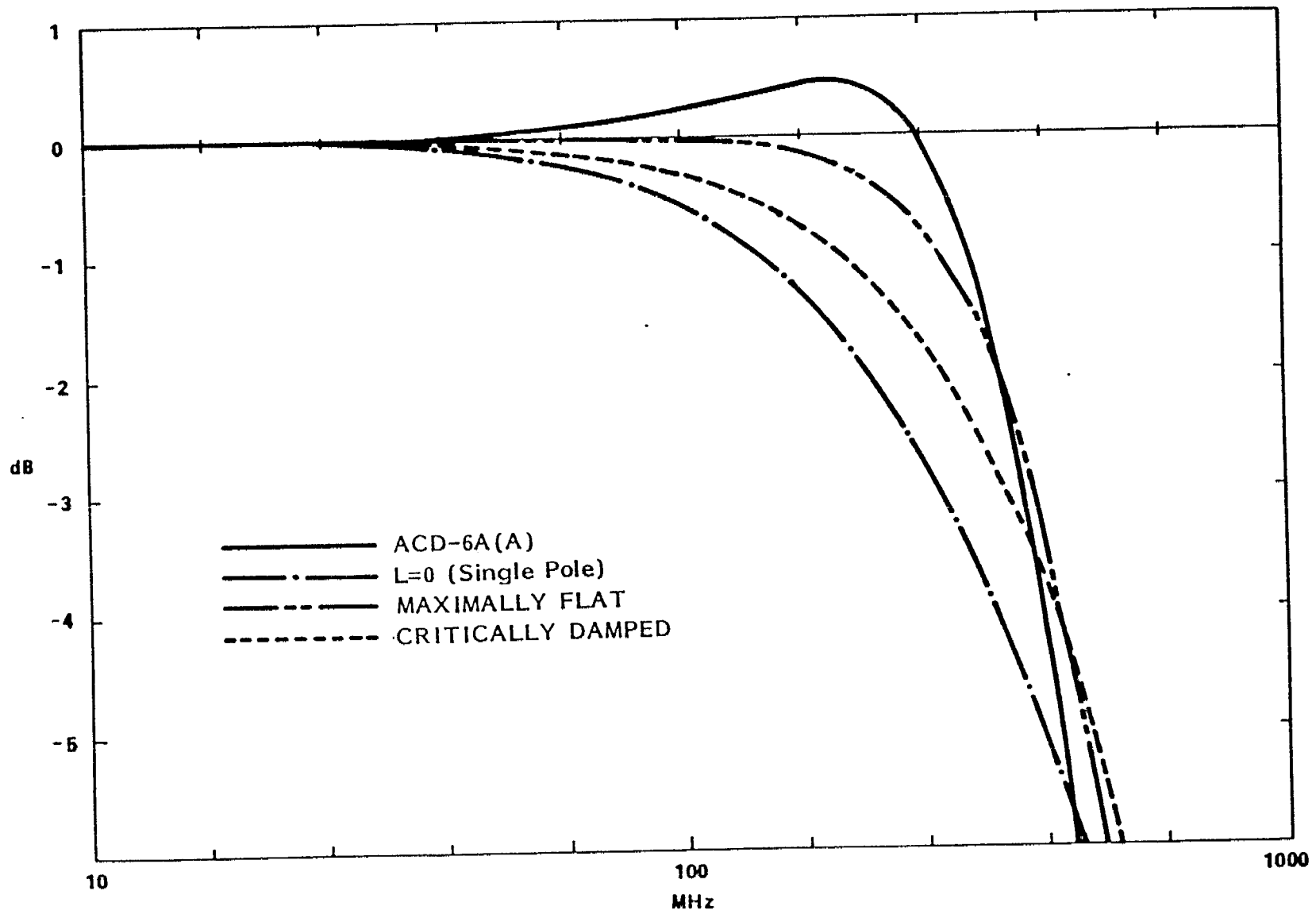


Figure 5. Equivalent Circuit Frequency Response as a Function of Inductance

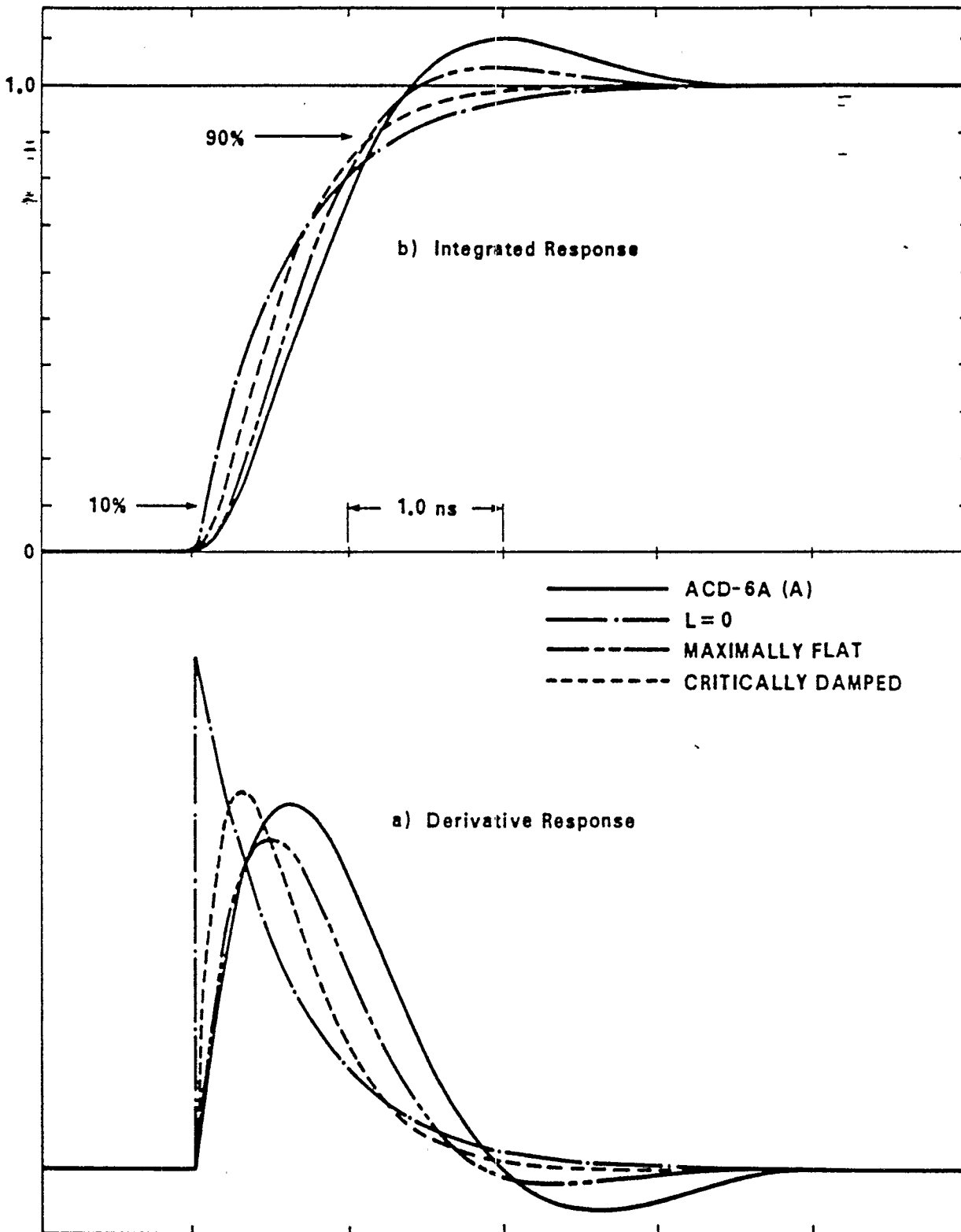


Figure 6. Equivalent Circuit Pulse Response as a Function of Inductance

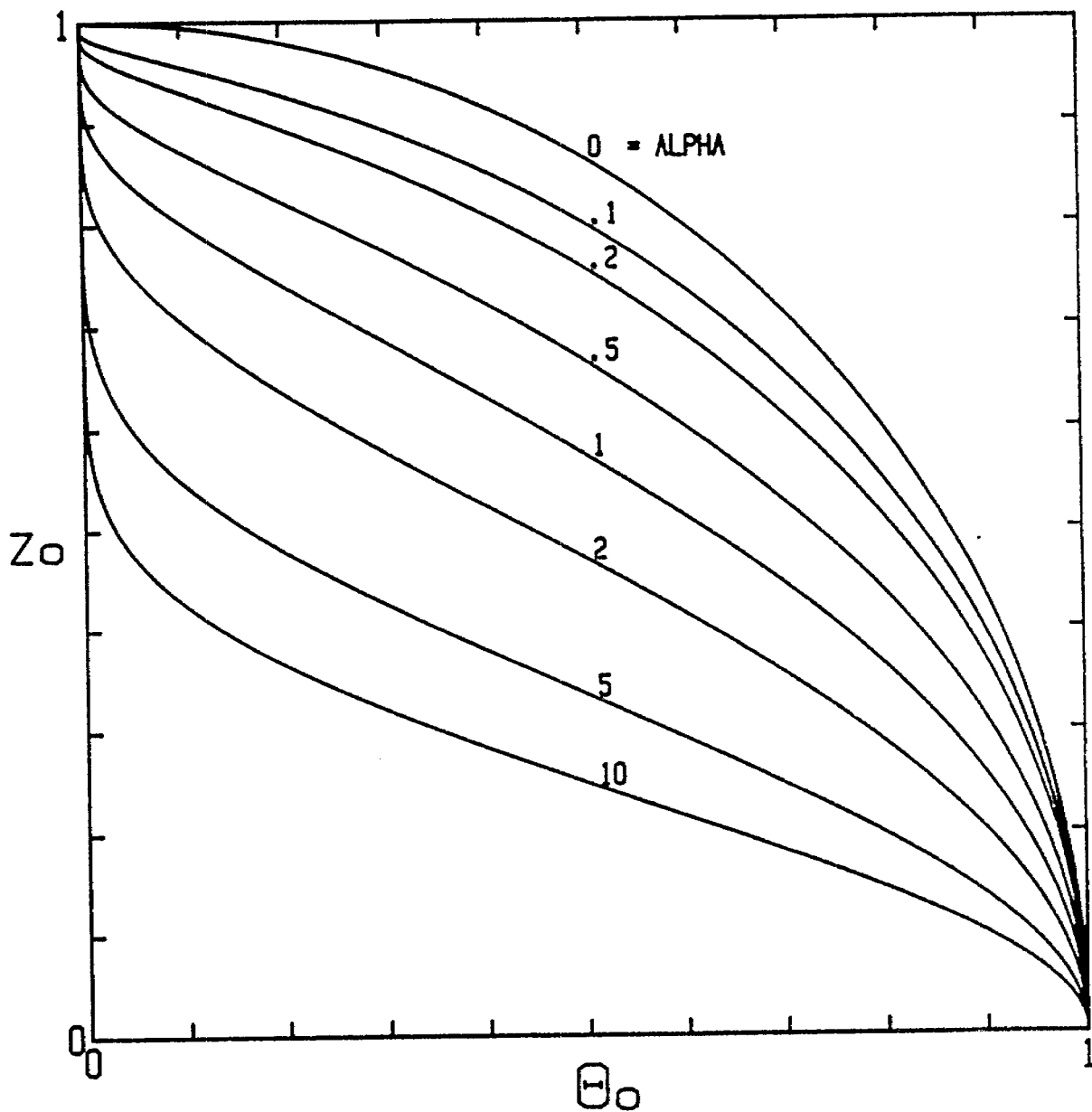


Figure 7. Equivalent Charge Heights

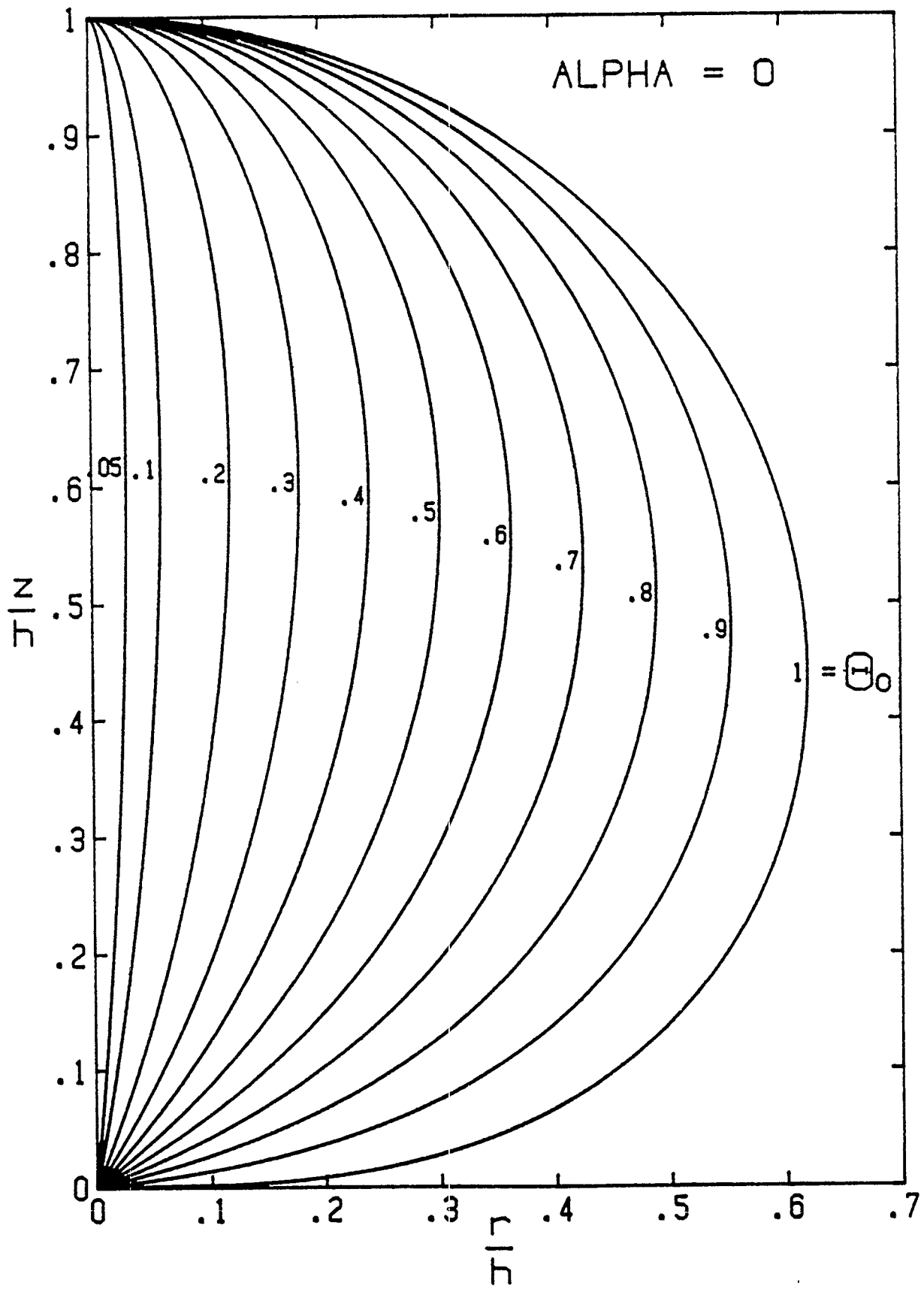


Figure 8. Antenna Contours for Various θ_0

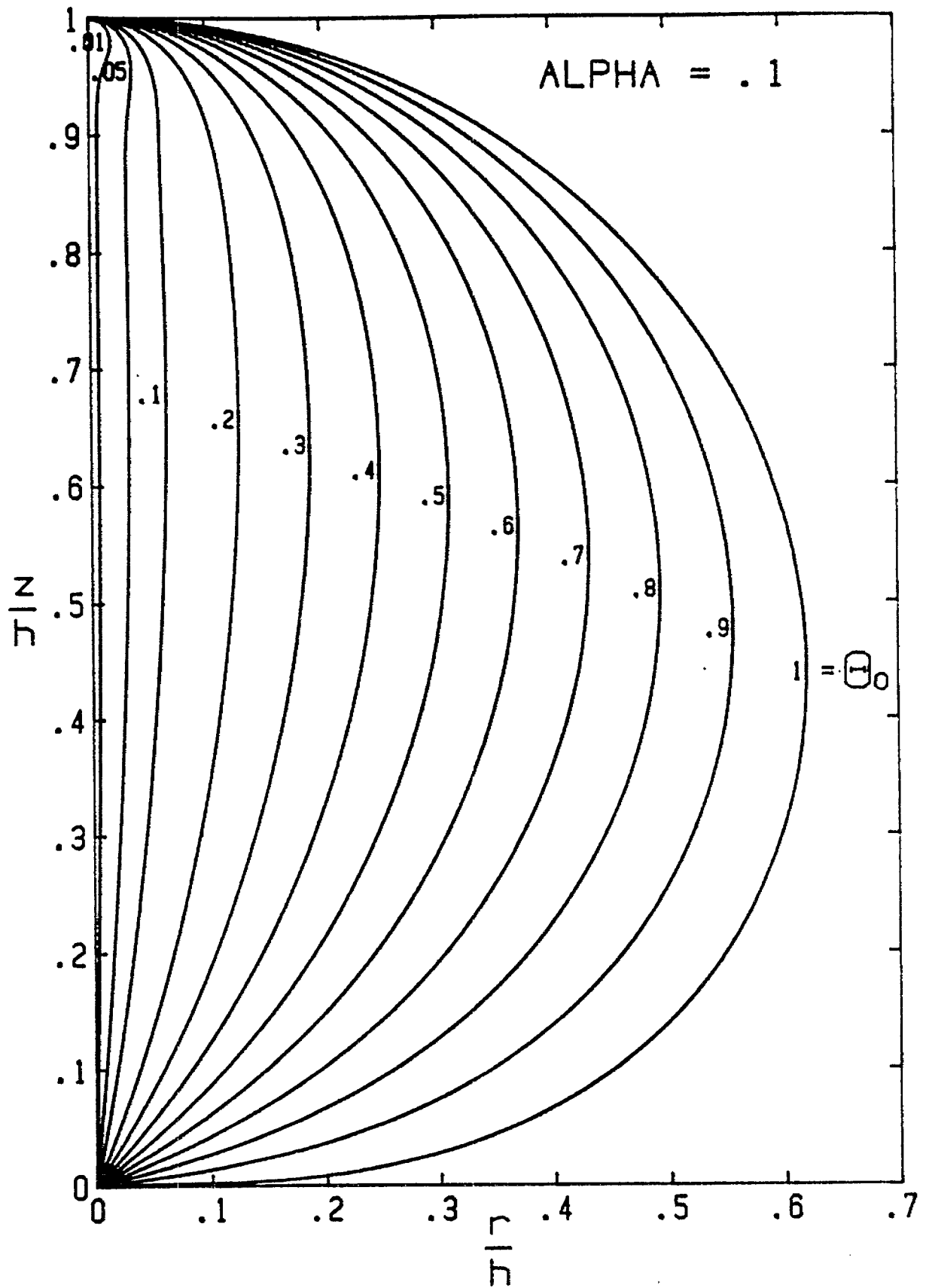


Figure 9. Antenna Contours for Various θ_0 .

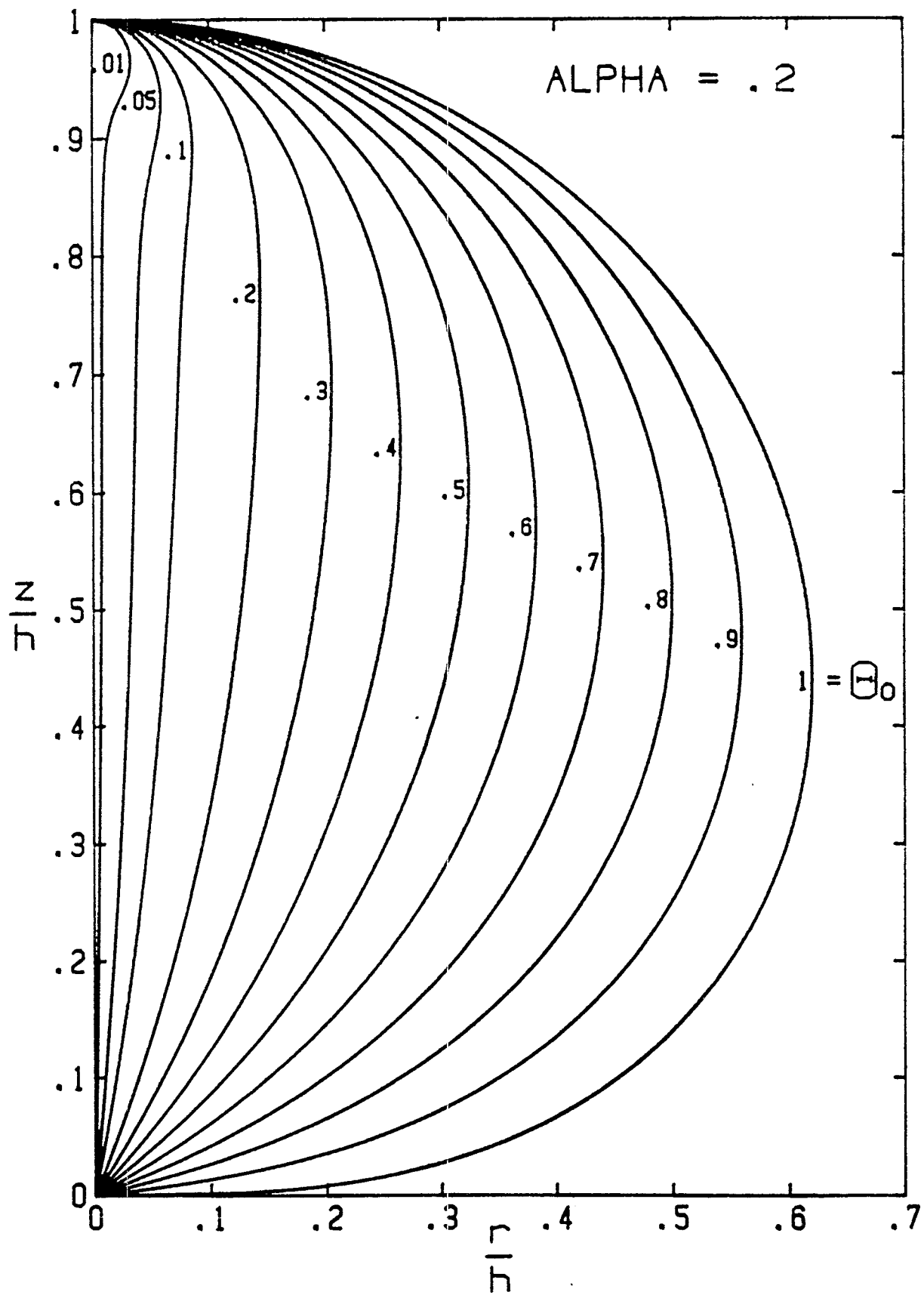


Figure 10. Antenna Contours for Various θ_0

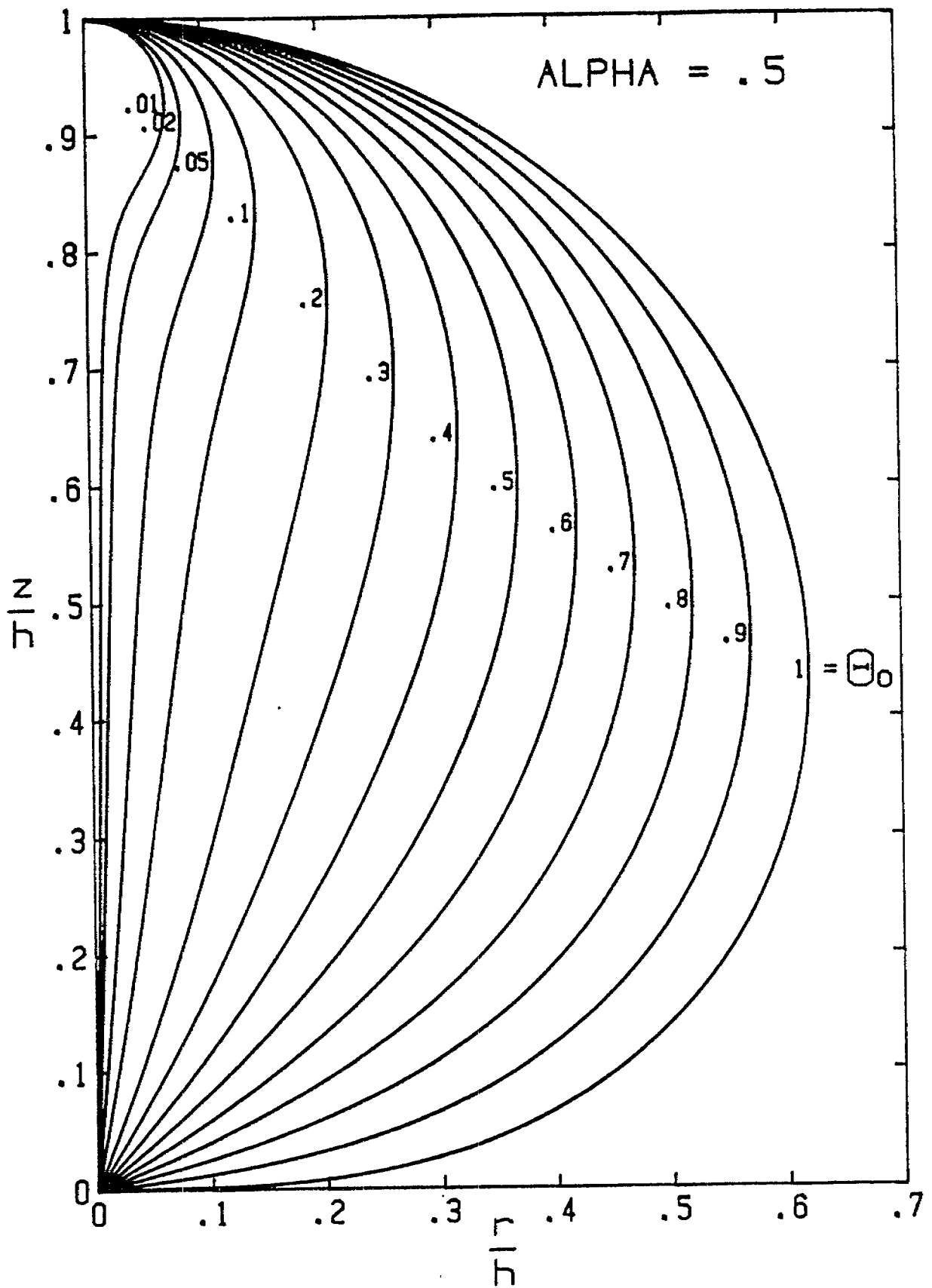


Figure 11. Antenna Contours for Various θ_0

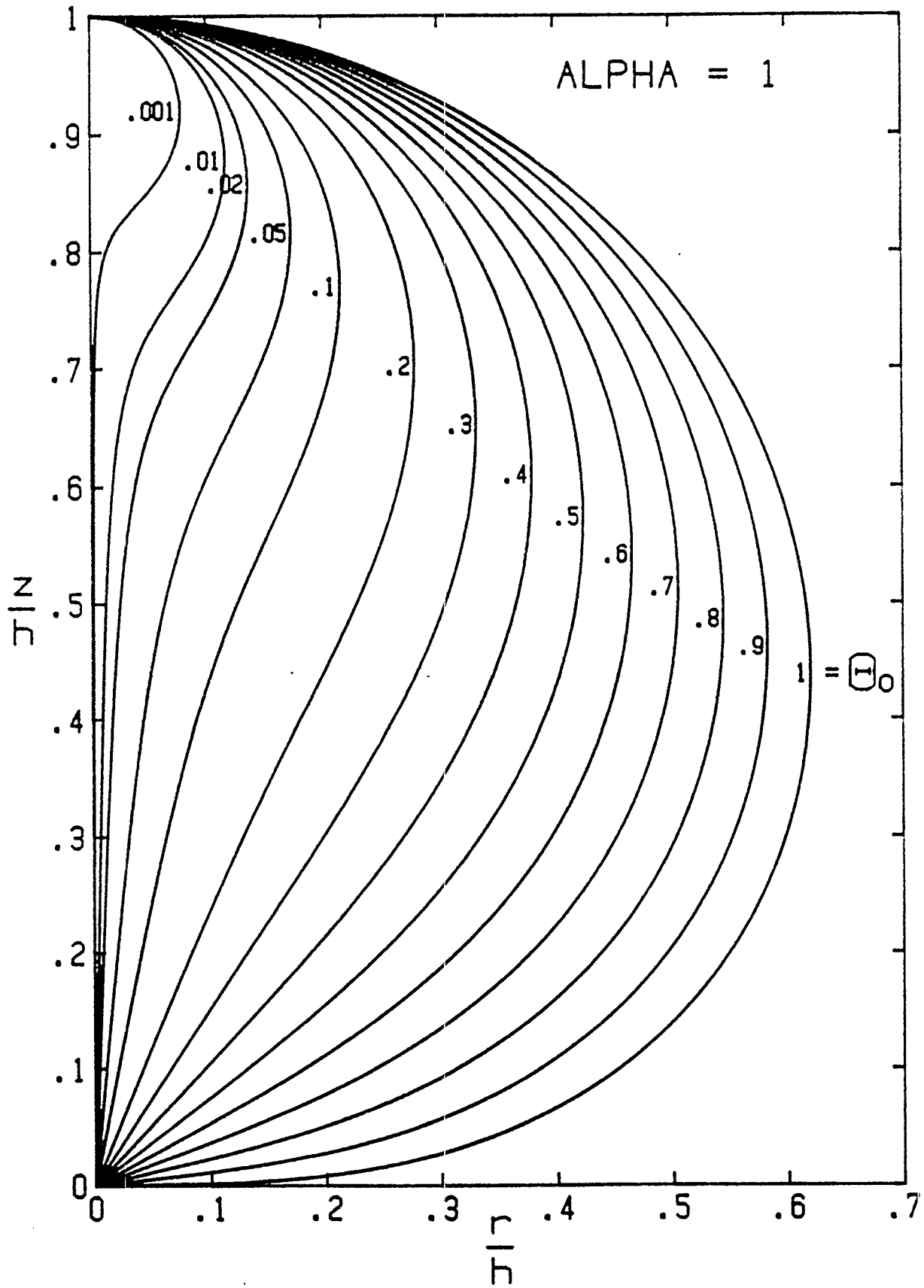


Figure 12. Antenna Contours for Various θ_0

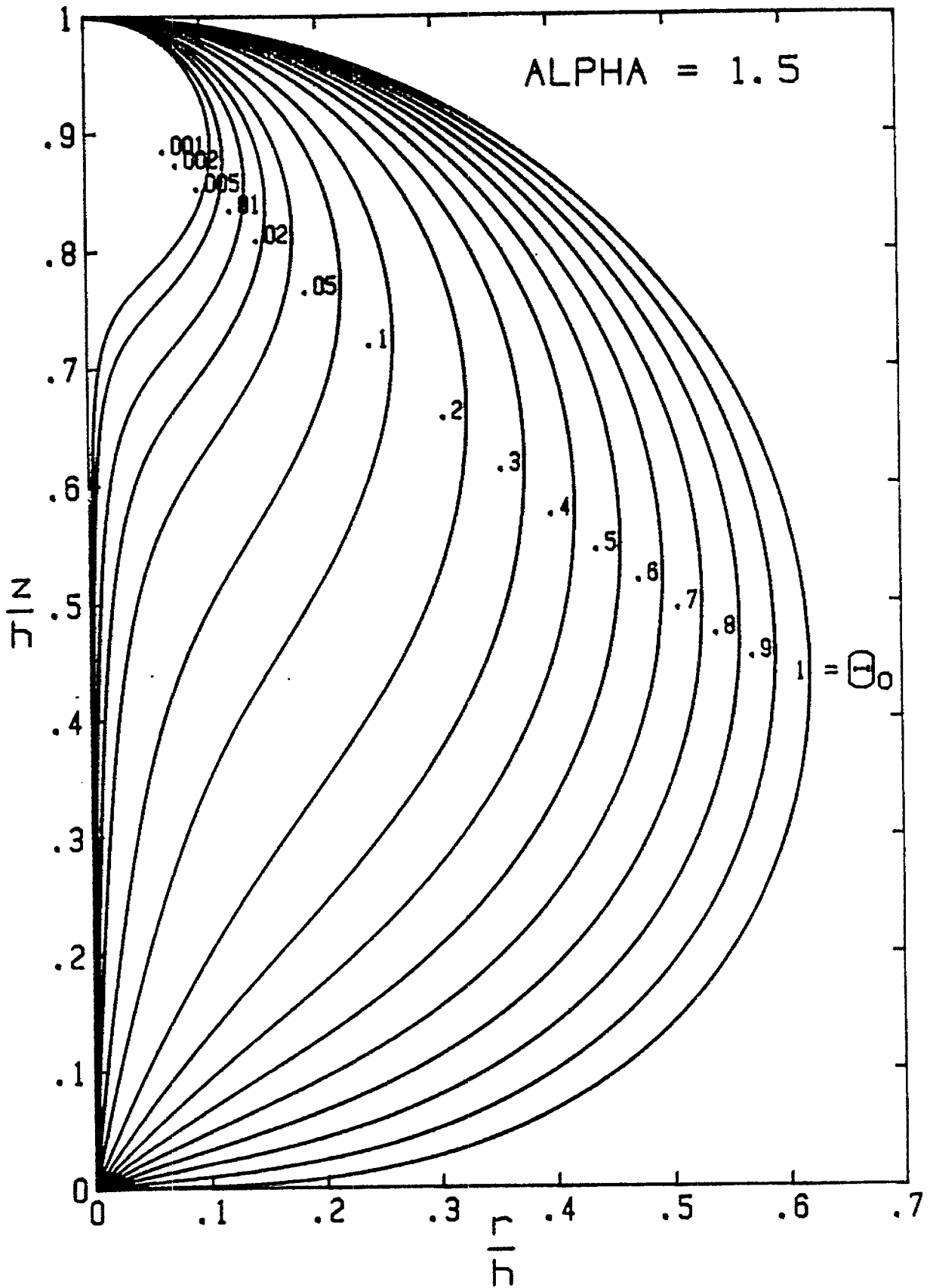


Figure 13. Antenna Contours for Various θ_0

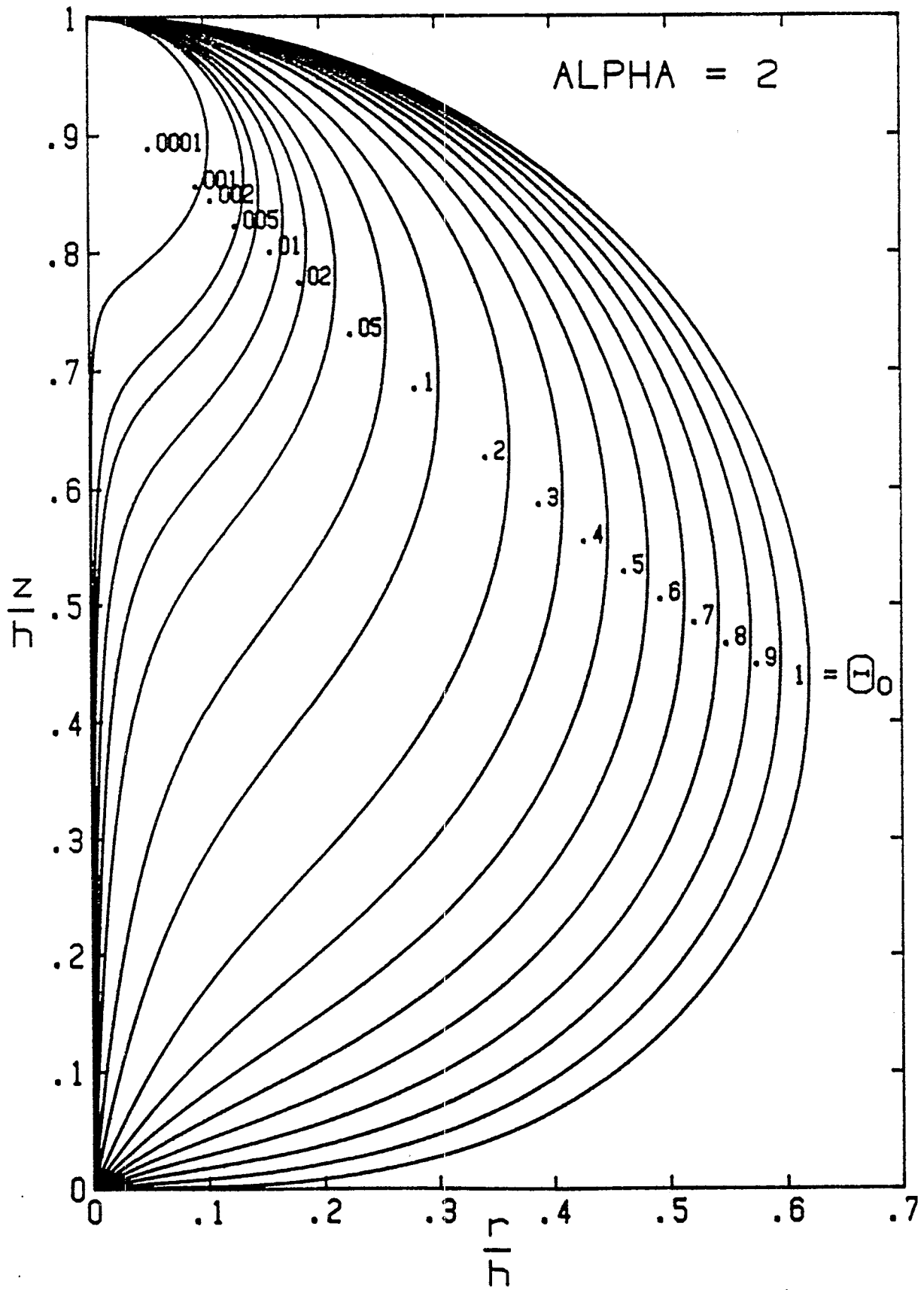


Figure 14. Antenna Contours for Various θ_0

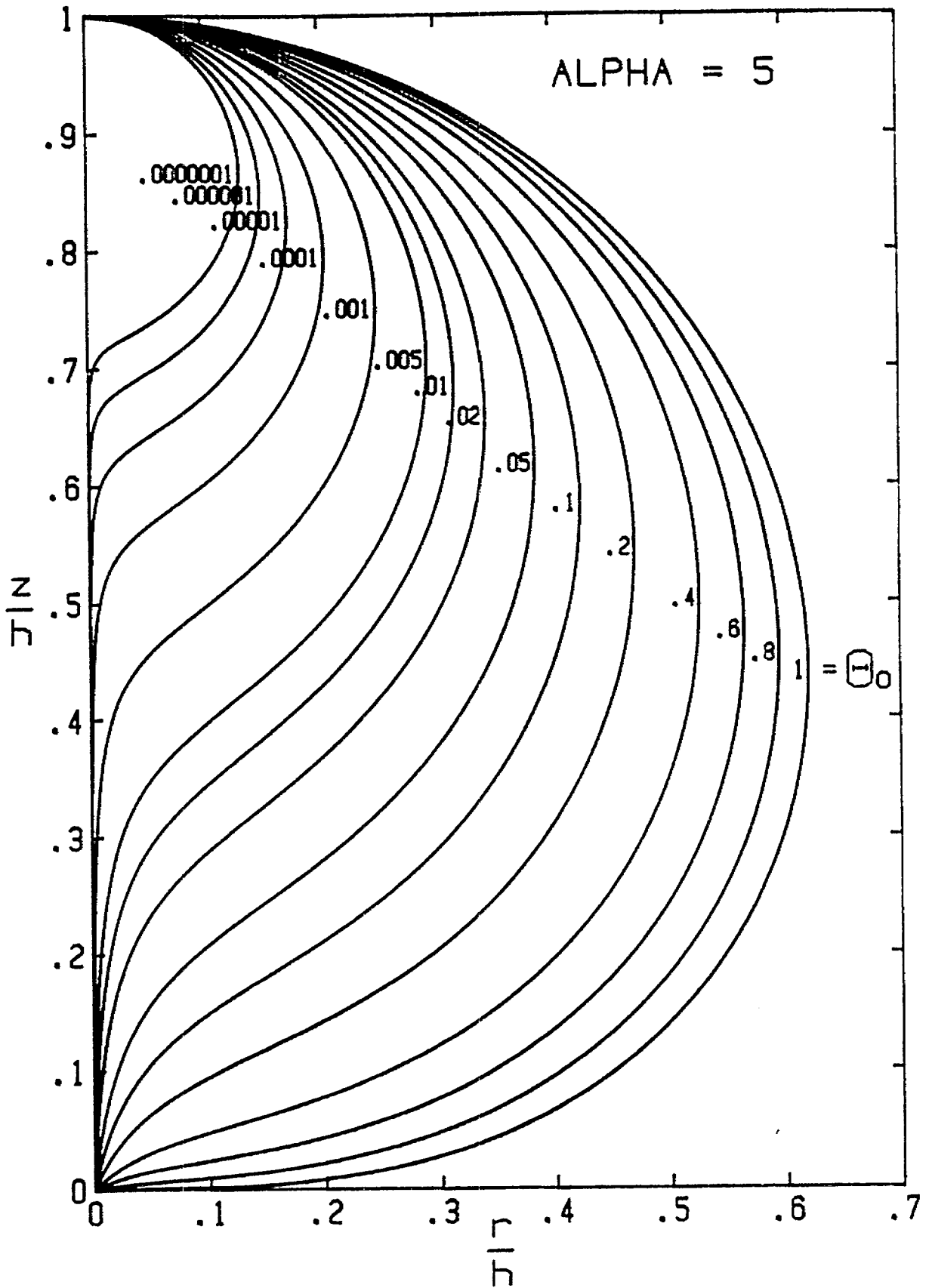


Figure 15. Antenna Contours for Various θ_0

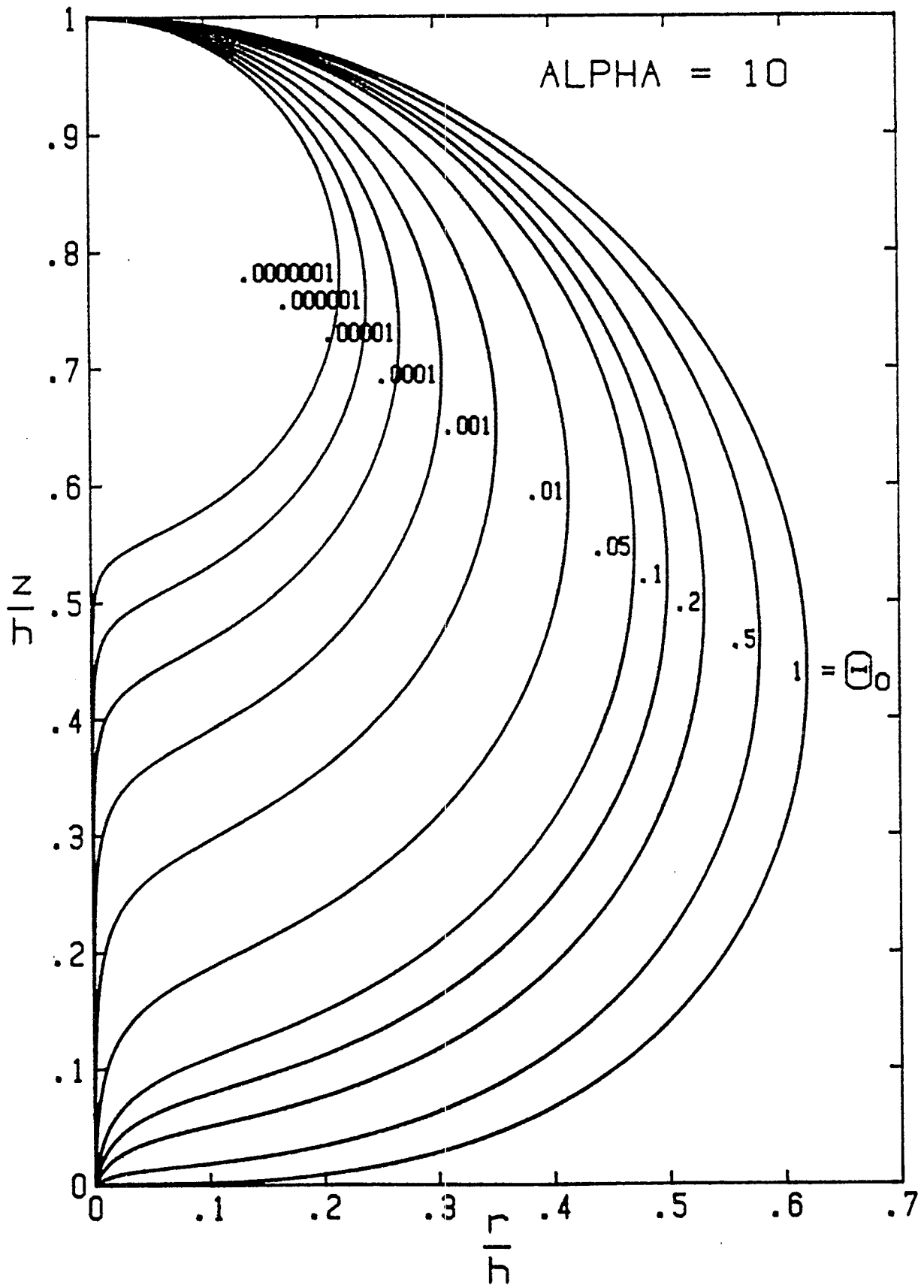


Figure 16. Antenna Contours for Various θ_0

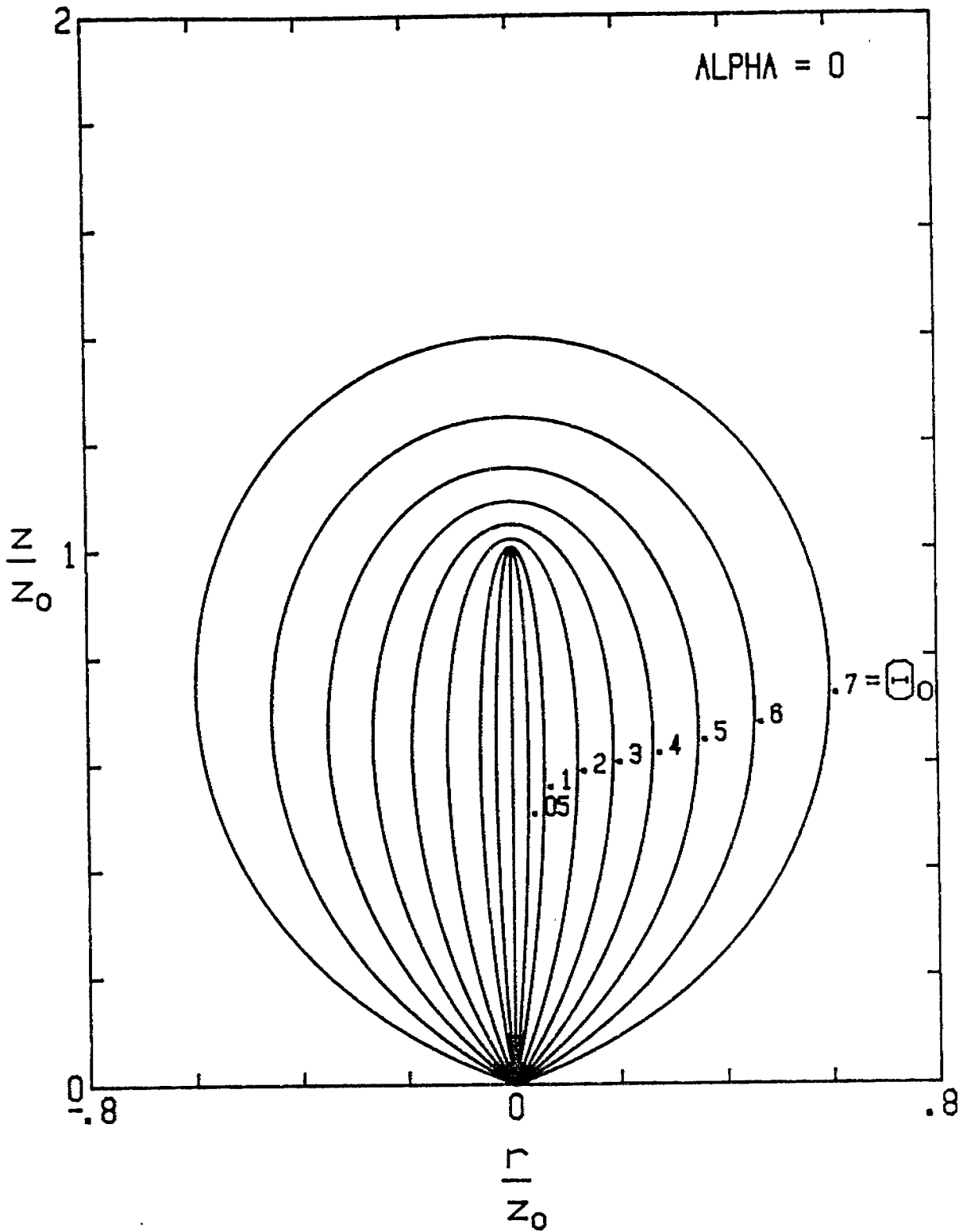


Figure 17. Equipotential Contours

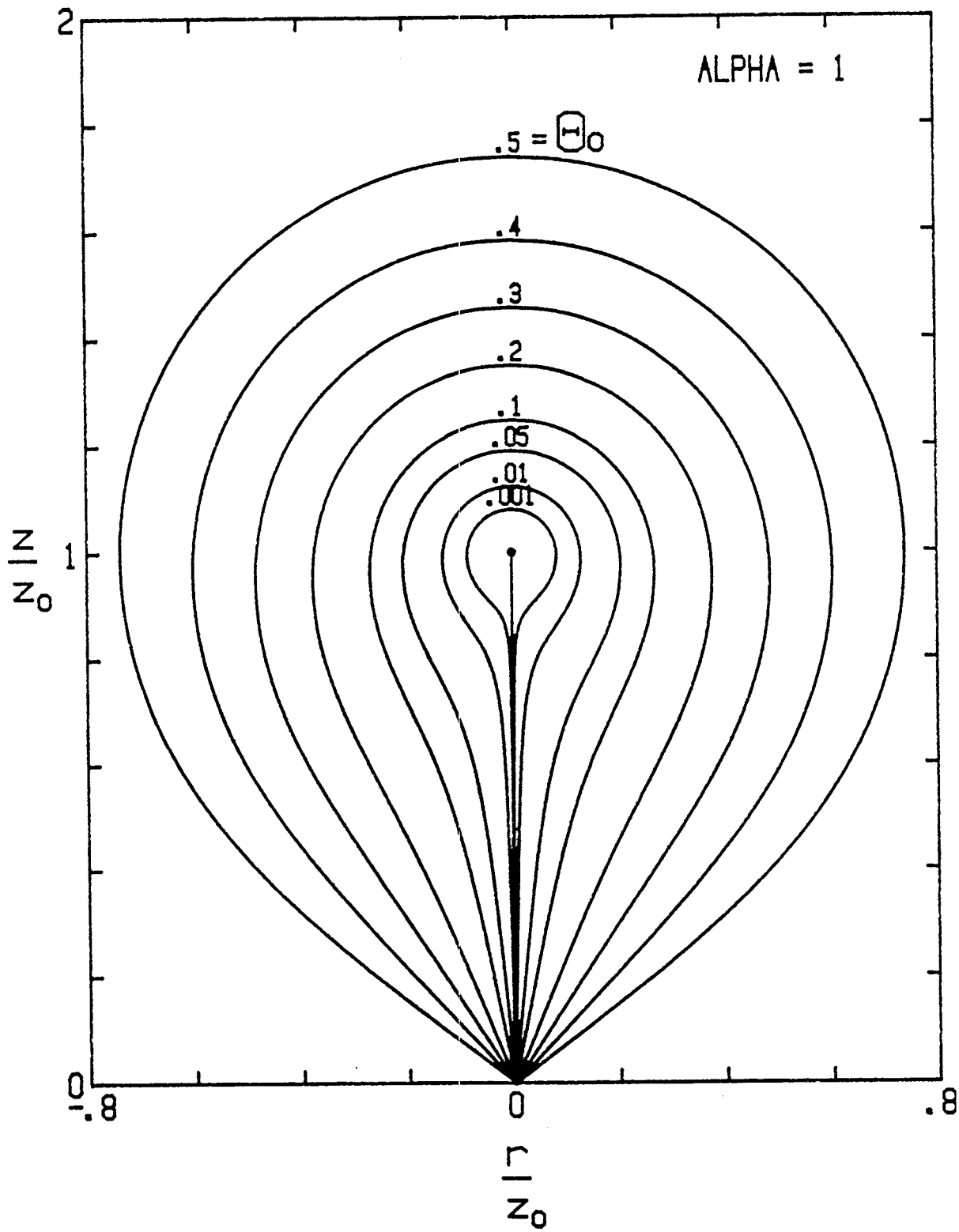


Figure 18. Equipotential Contours

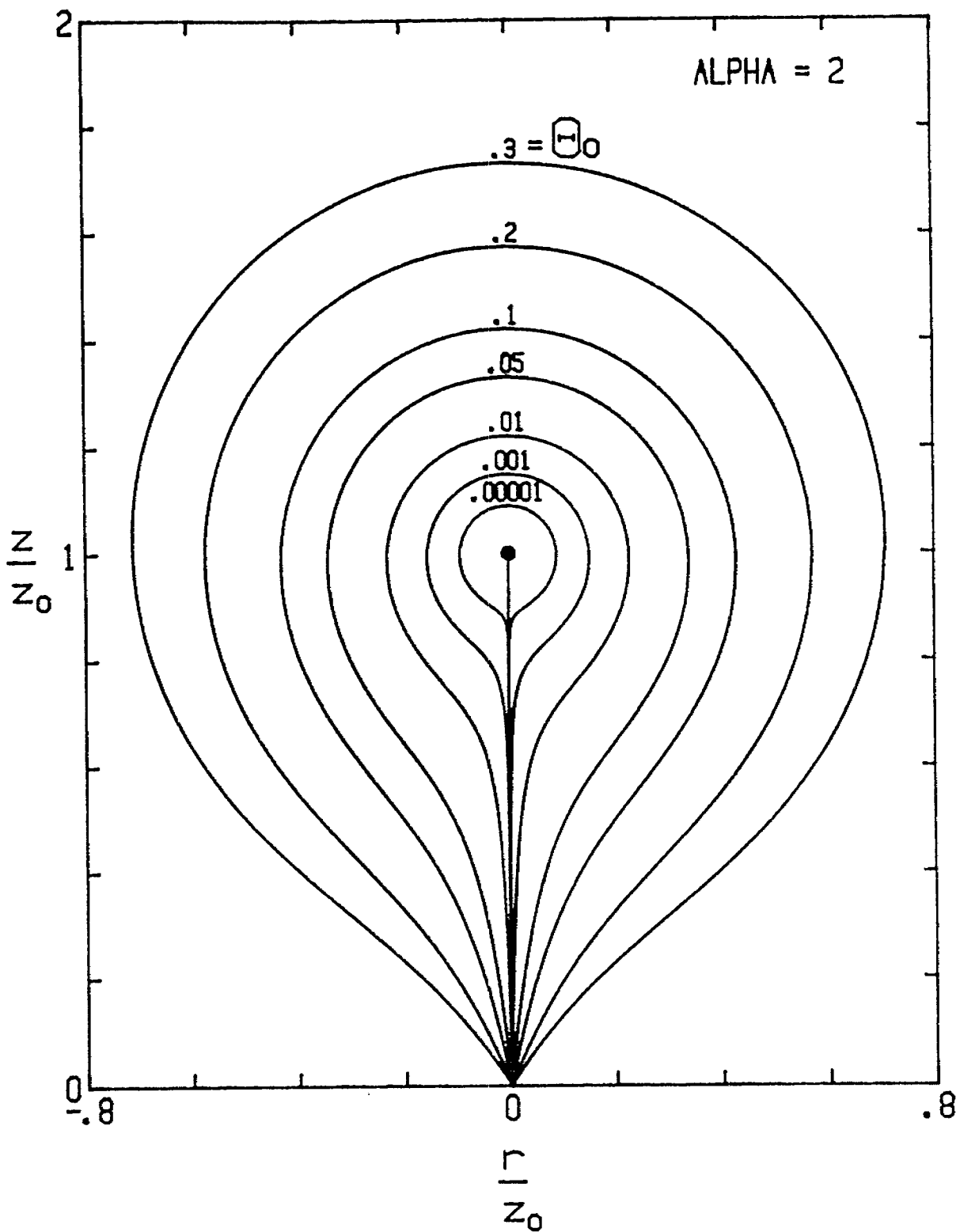


Figure 19. Equipotential Contours

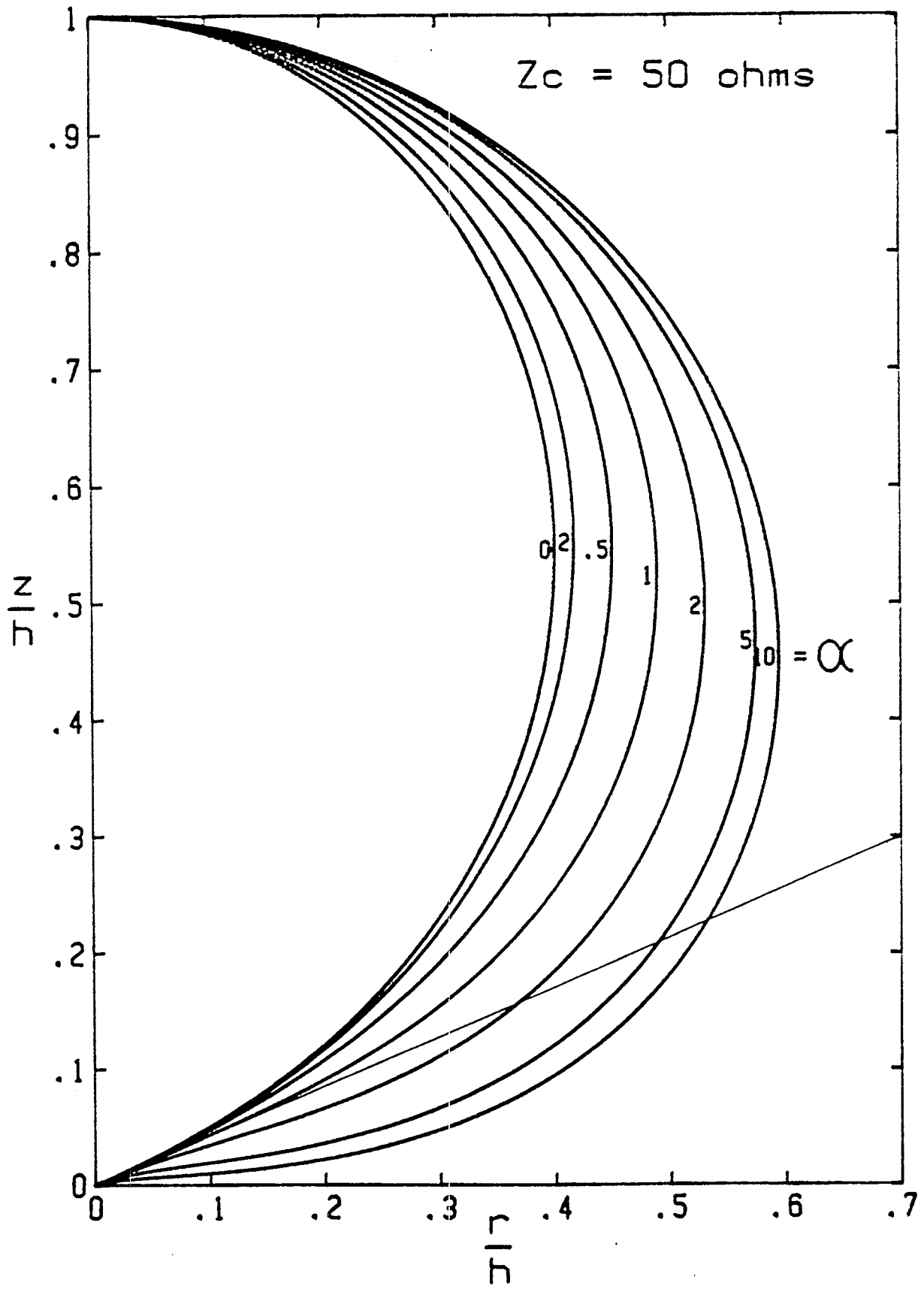


Figure 20. Antenna Contours for Various α

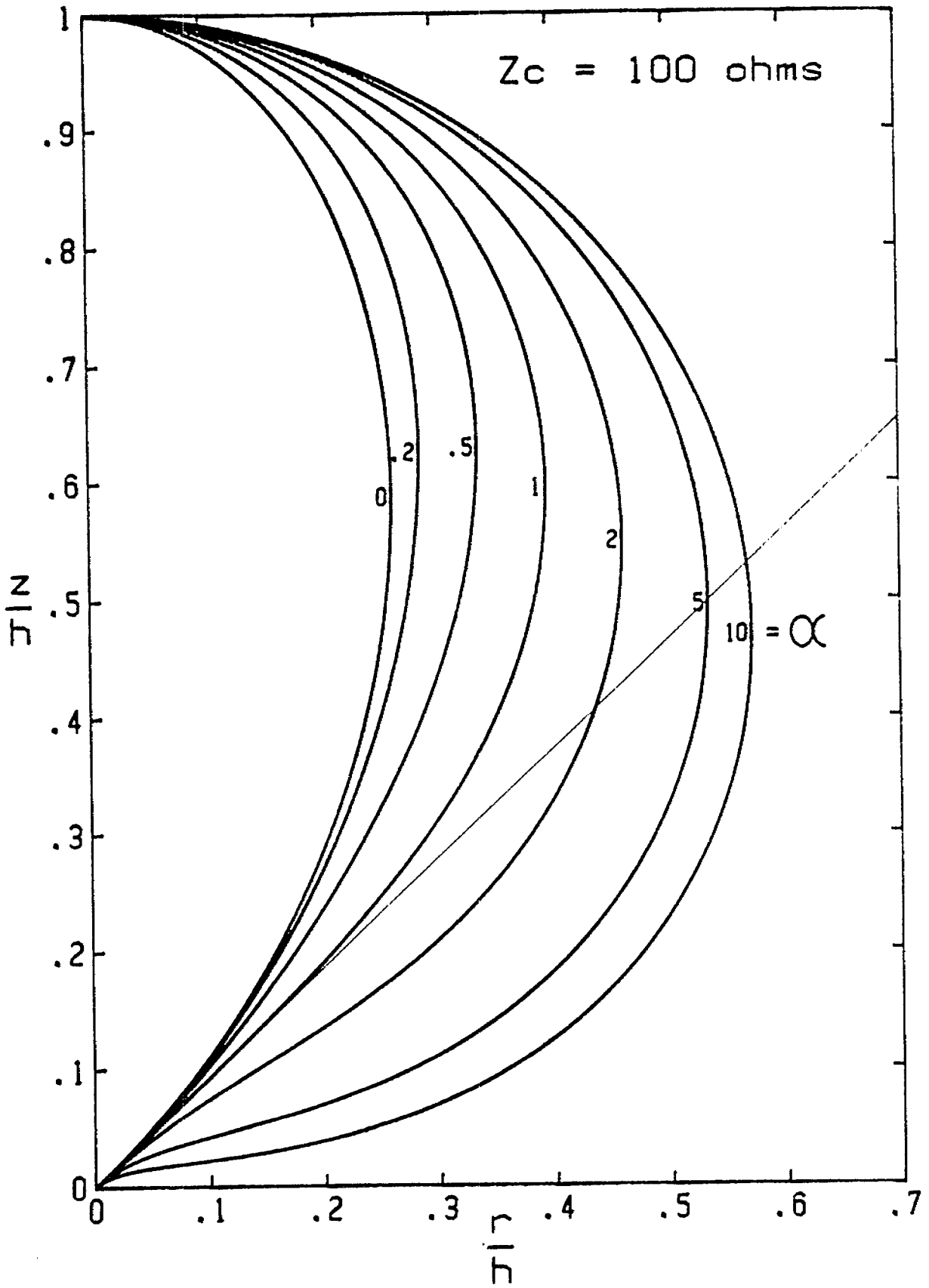


Figure 21. Antenna Contours for Various α

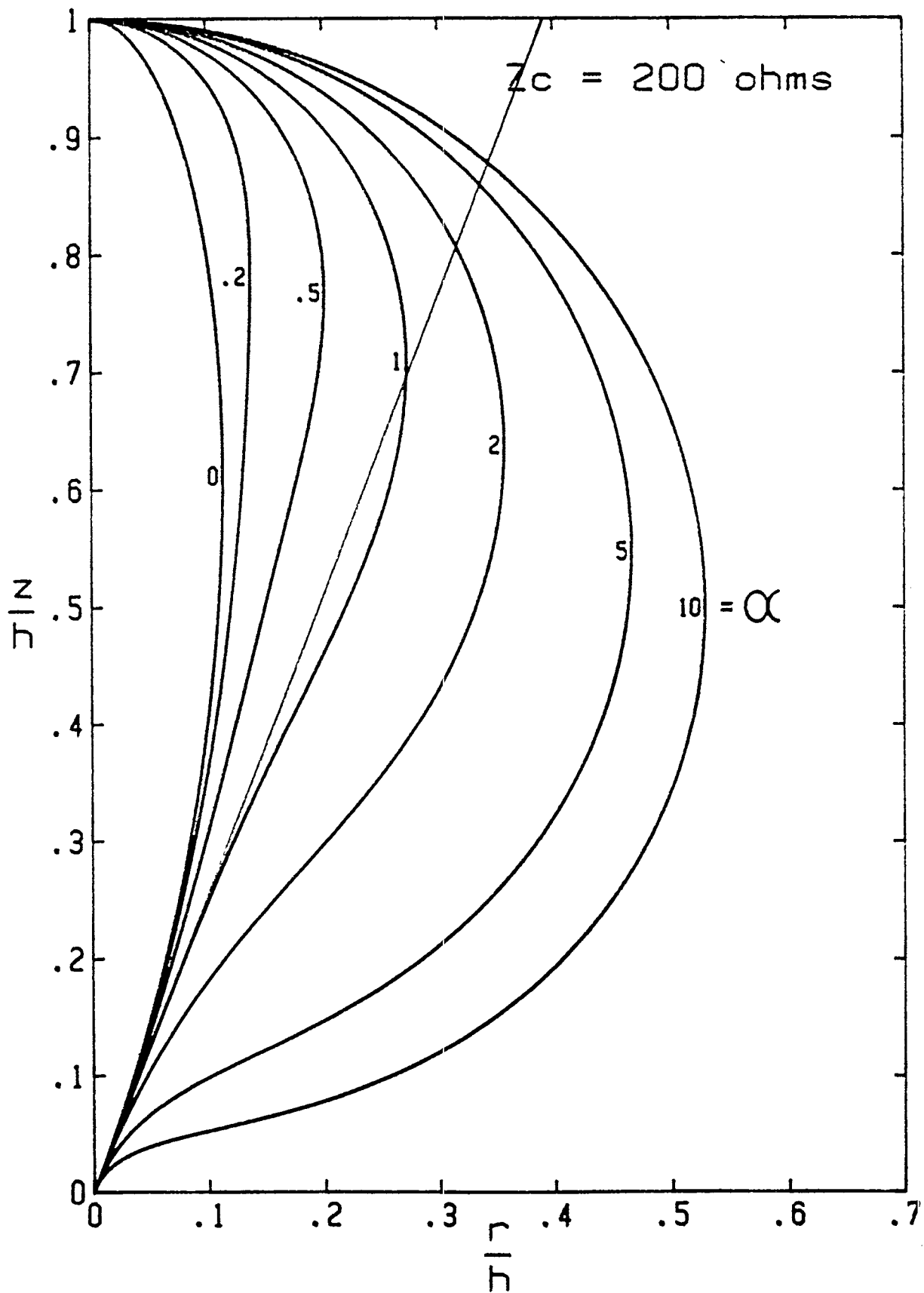


Figure 22. Antenna Contours for Various α

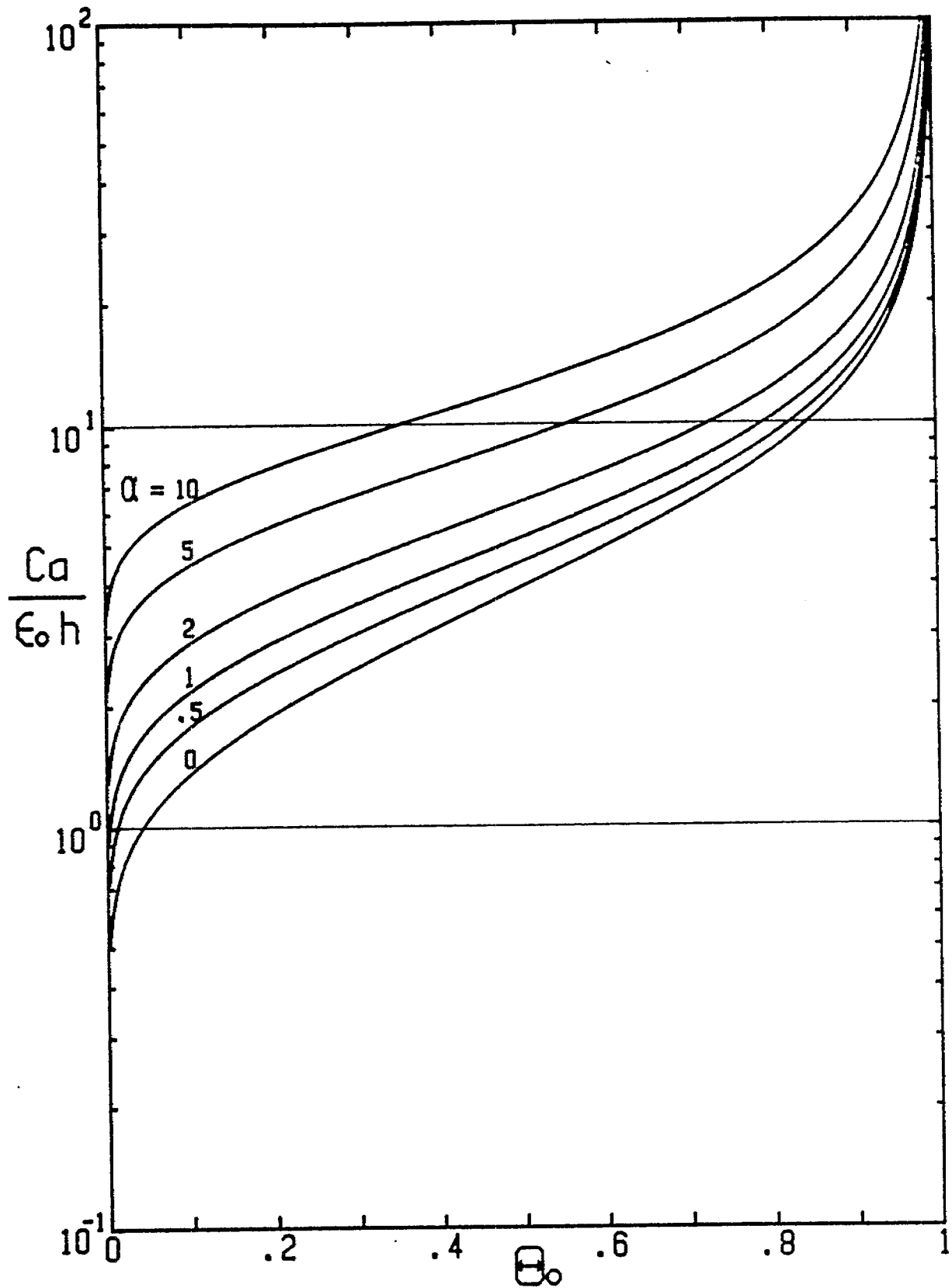


Figure 23. Normalized Antenna Capacitance

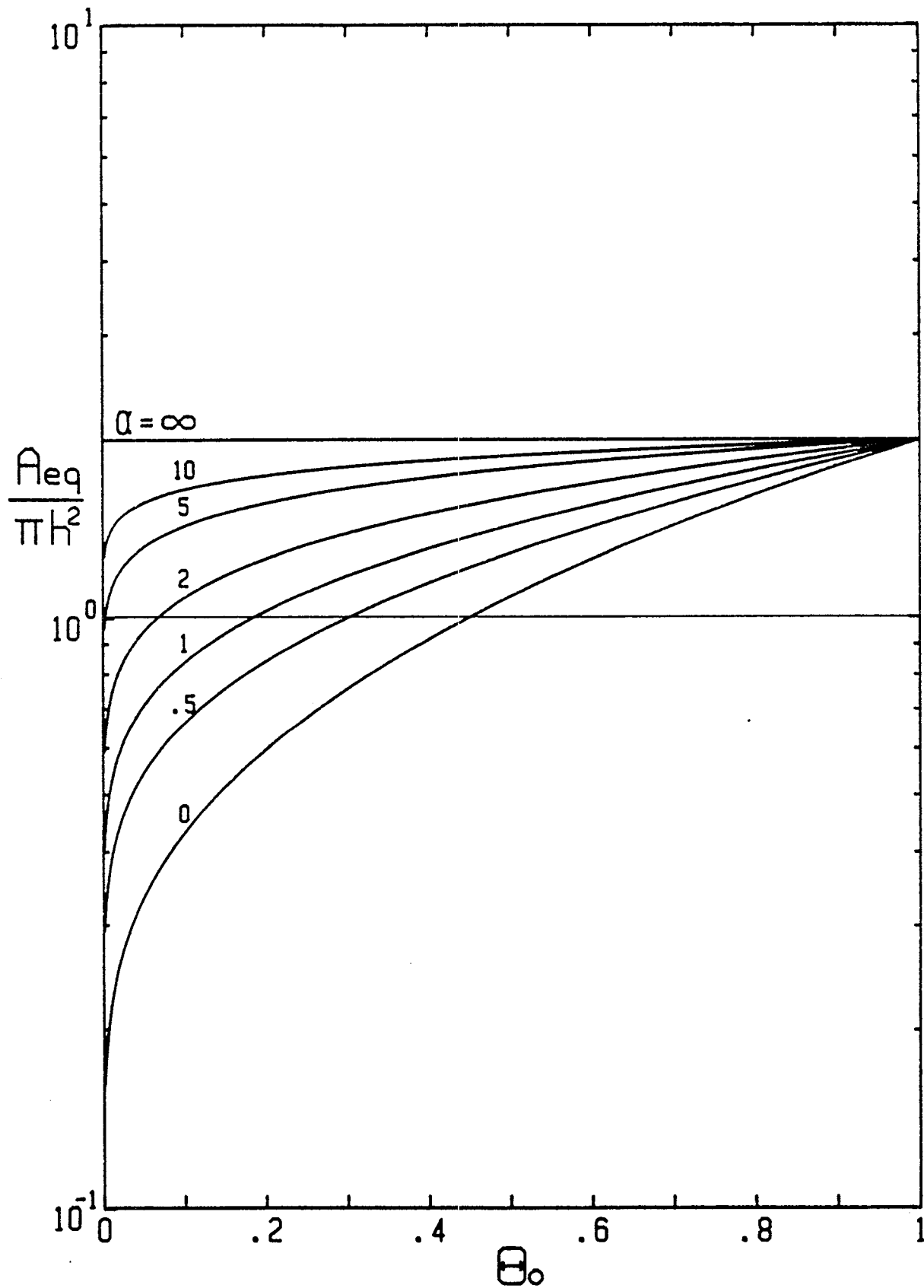


Figure 24. Normalized Antenna Sensitivity

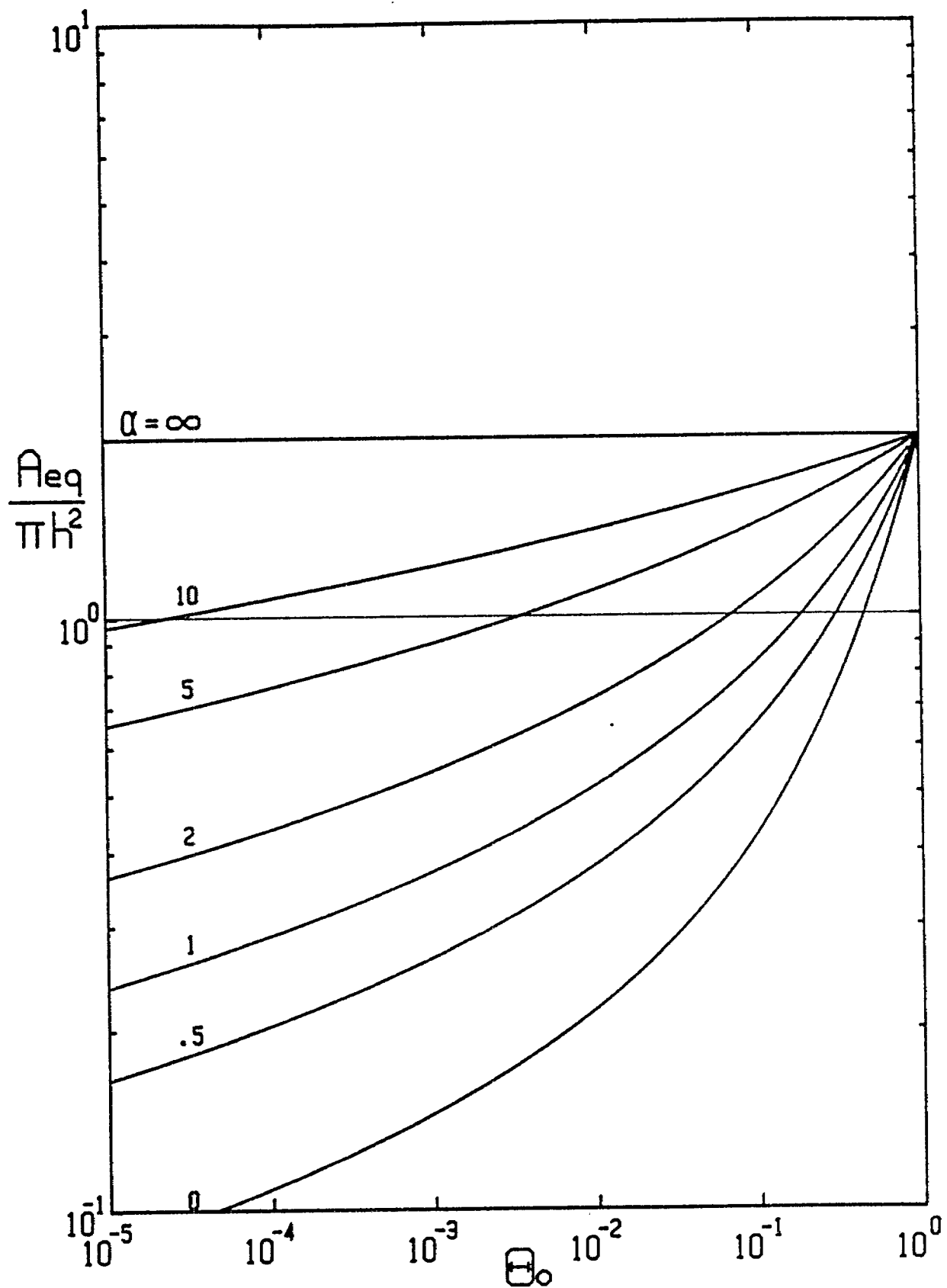


Figure 25. Normalized Antenna Sensitivity

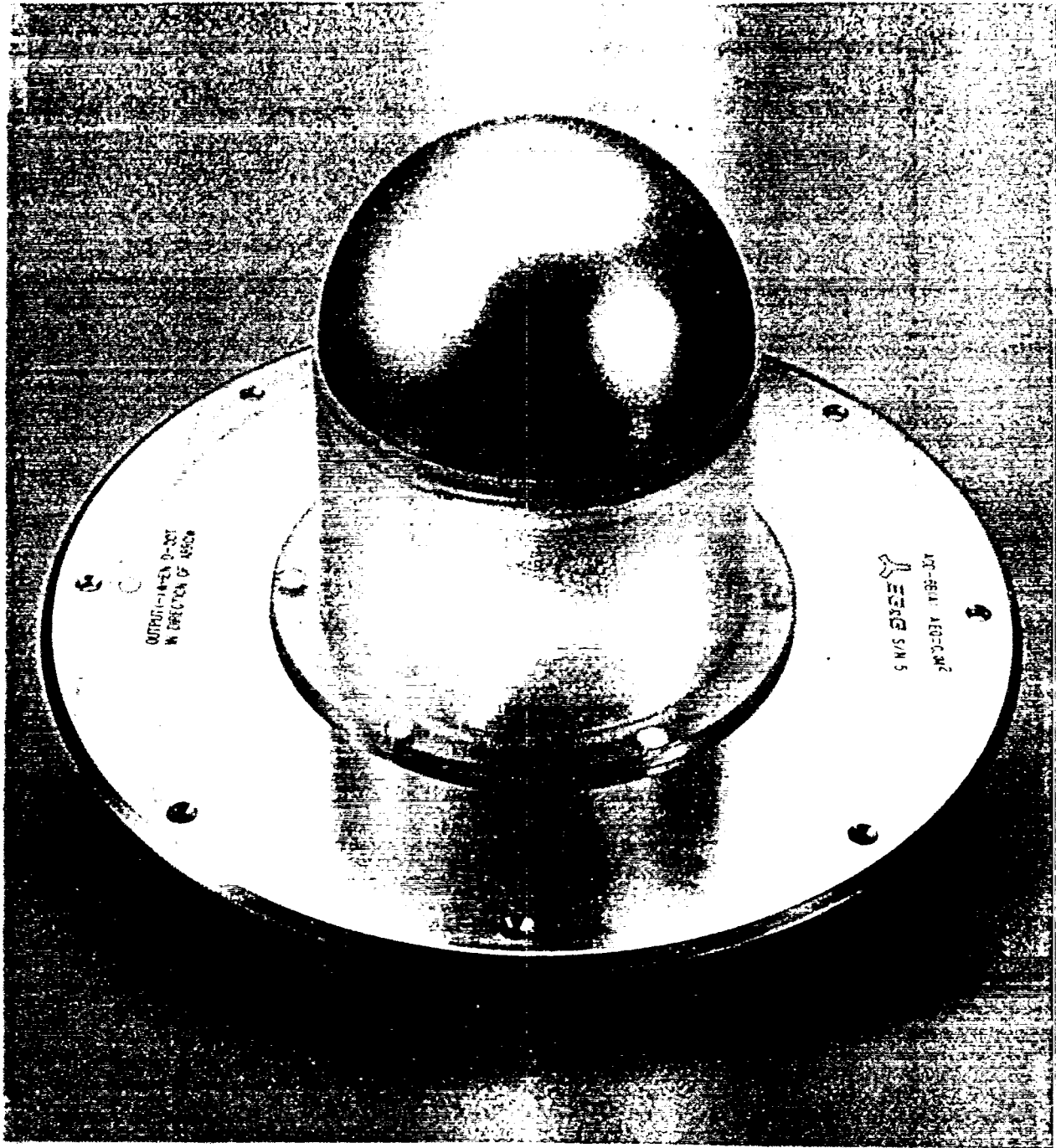


Figure 26. ACD-6B(A) Sensor with New Shape

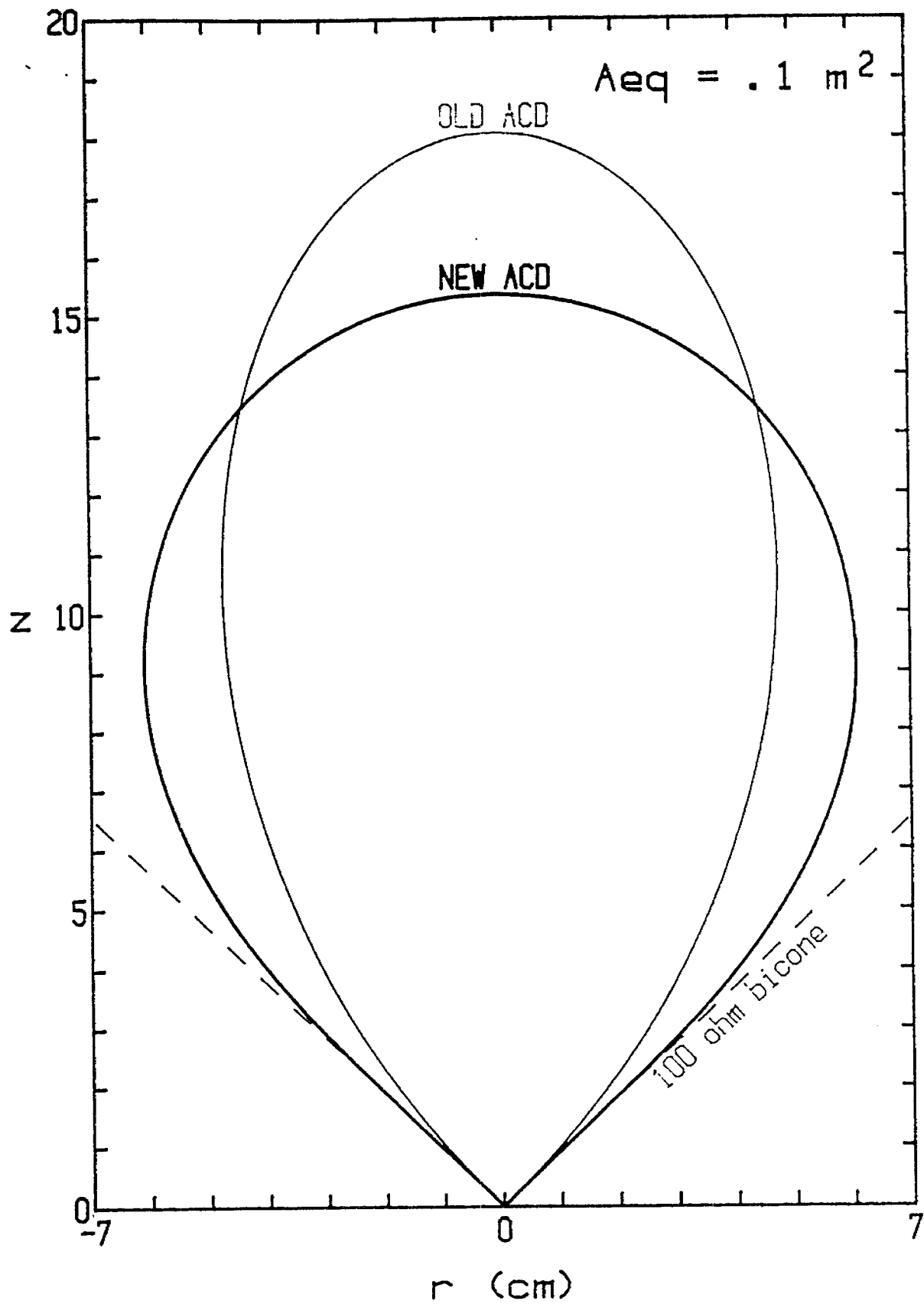


Figure 27. ACD Element Shape Comparison

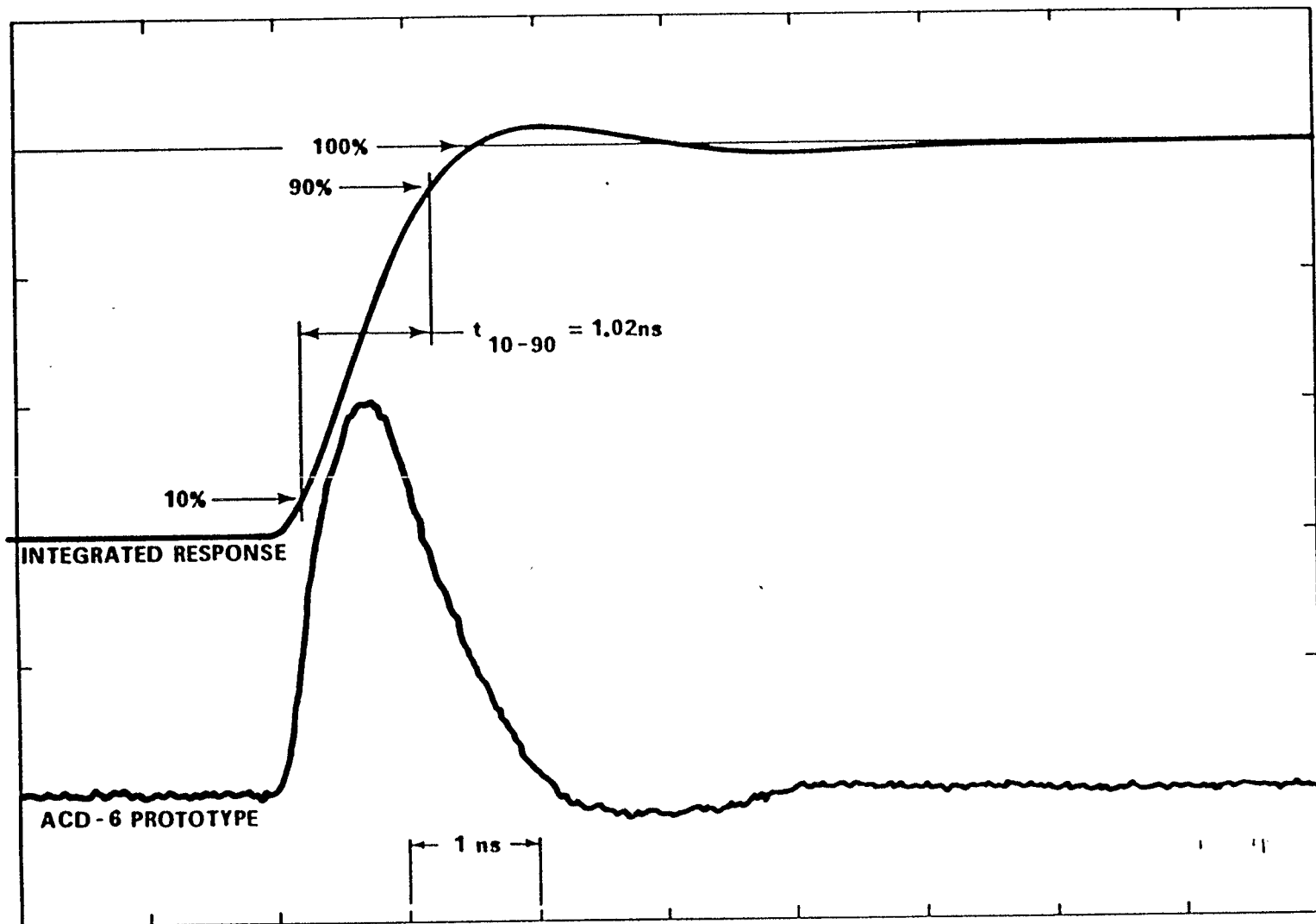


Figure 28. Pulse Response of ACD-6B(A)

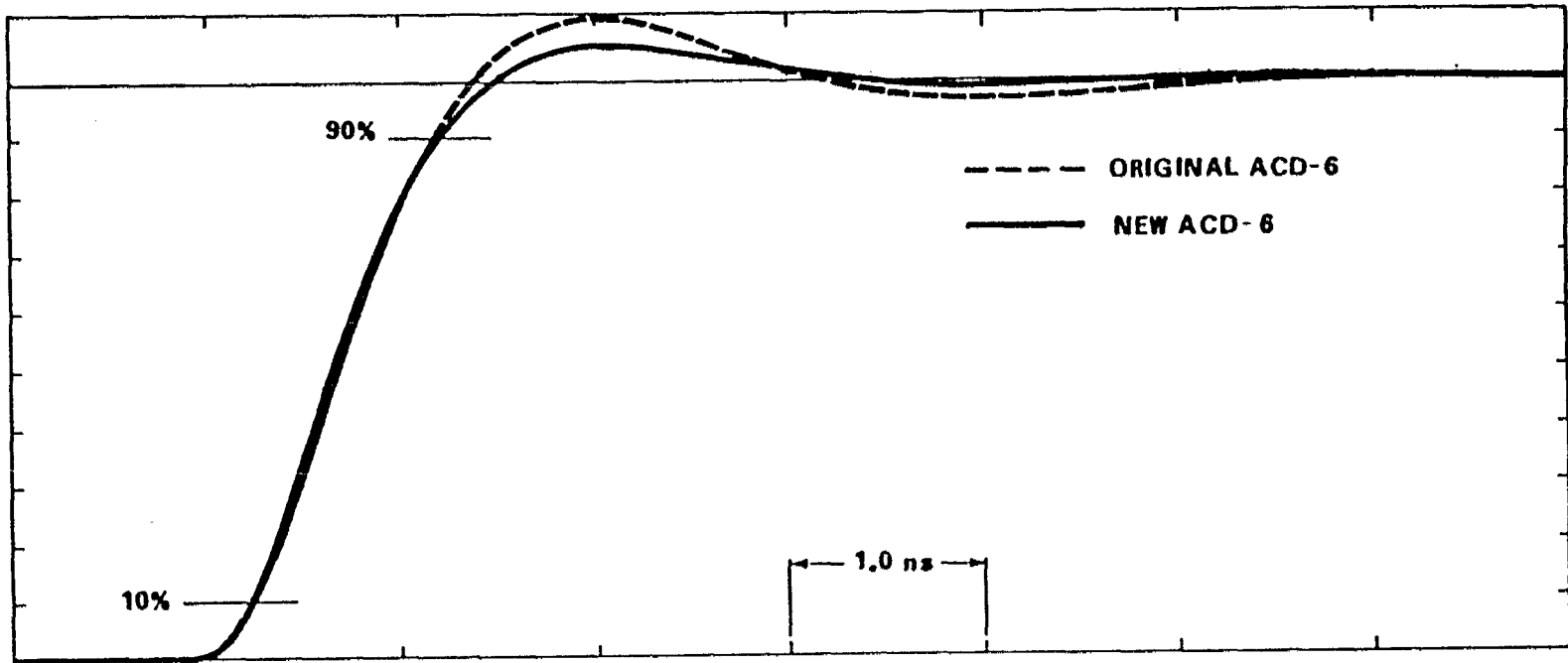
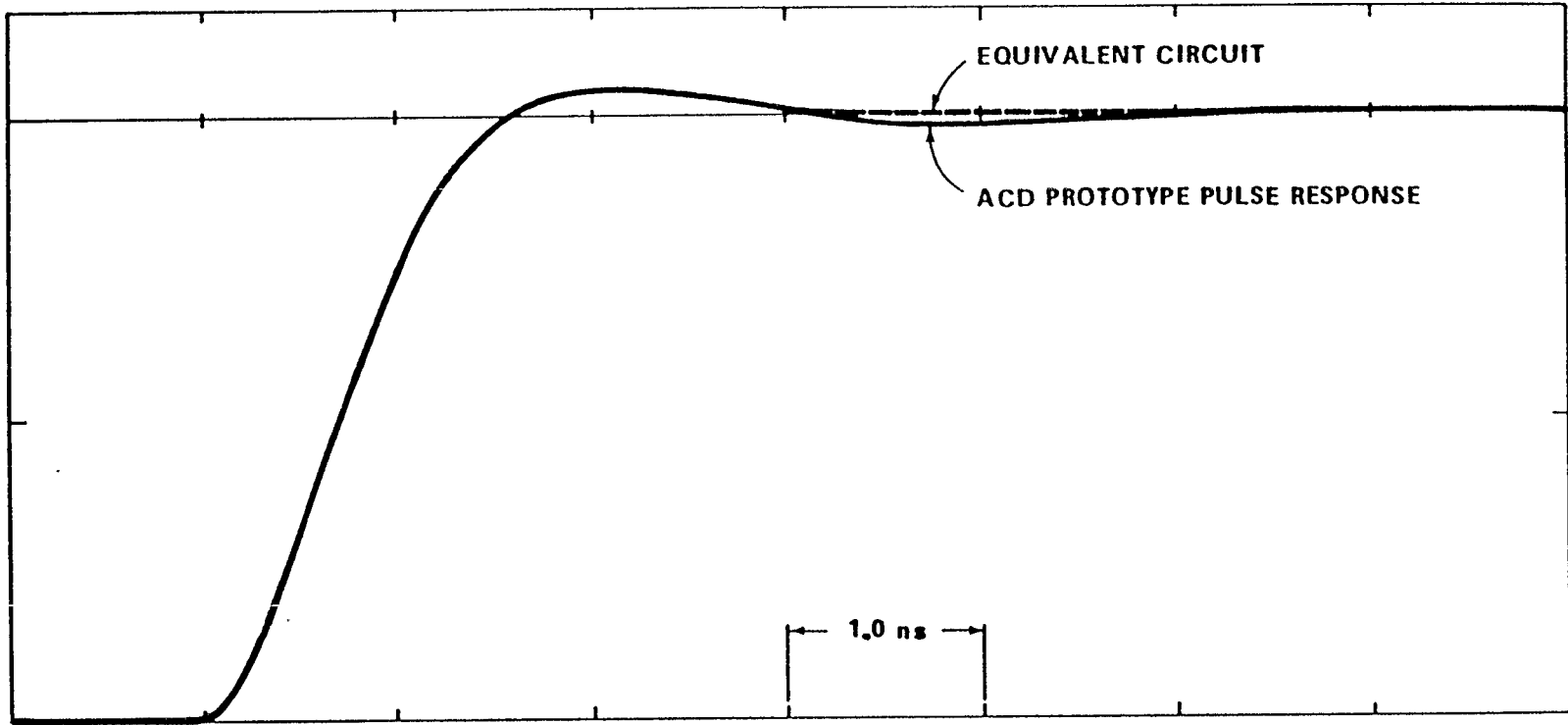
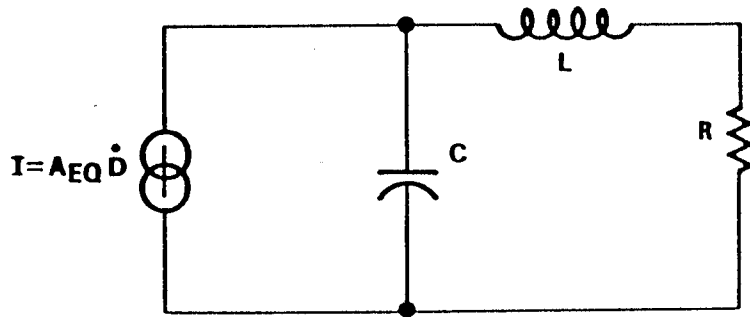


Figure 29. Comparison of Old and New ACD-6 Sensor Pulse Response



EQUIVALENT CIRCUIT OF NEW ACD SENSOR



C = Element Capacitance = 13.5pF
 L = Element Inductance = 17nH
 R = Load Resistance = 50Ω

Figure 30. New ACD-6 Equivalent Circuit and Pulse Response Comparison

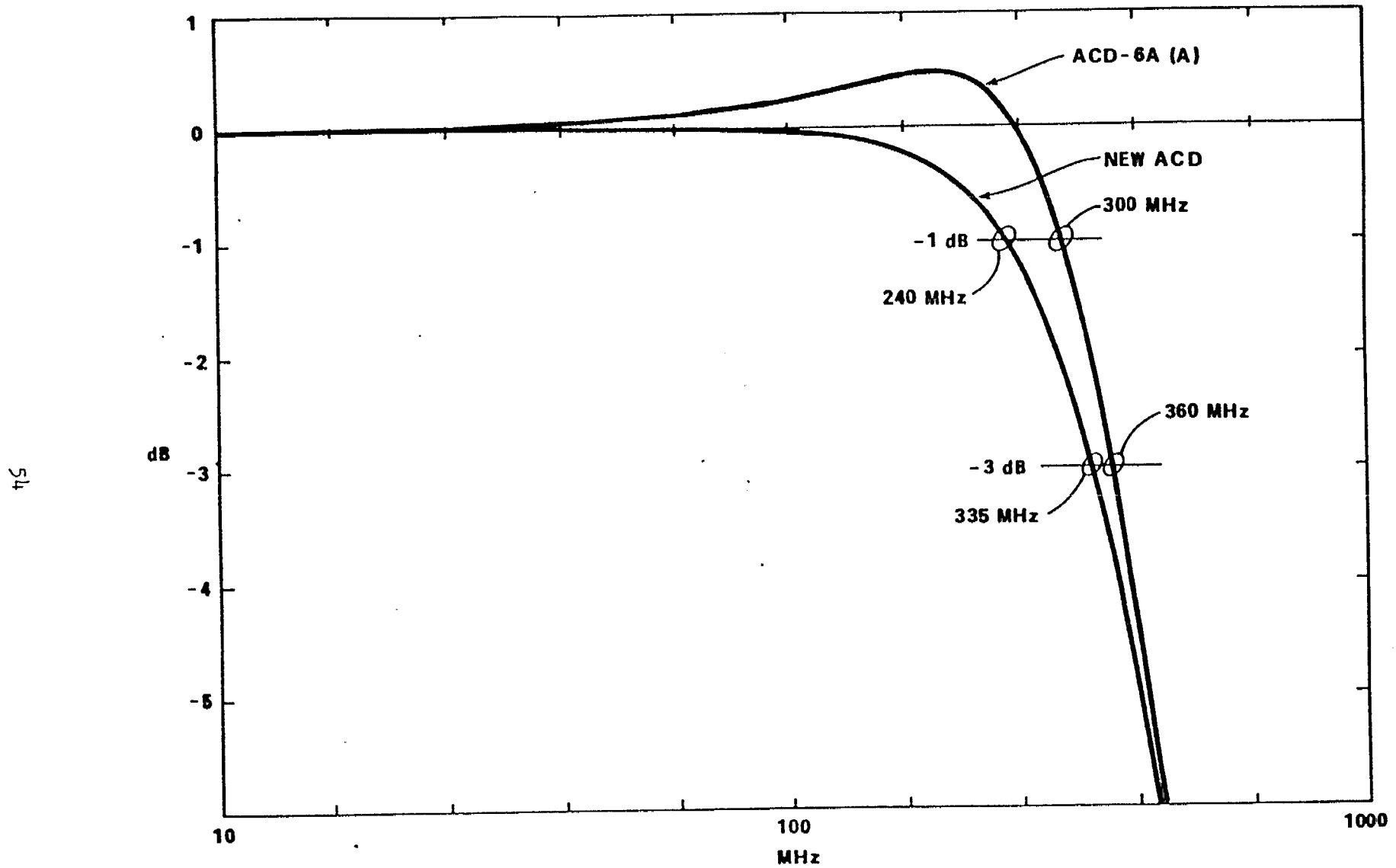


Figure 31. New ACD-6 Calculated Frequency Response

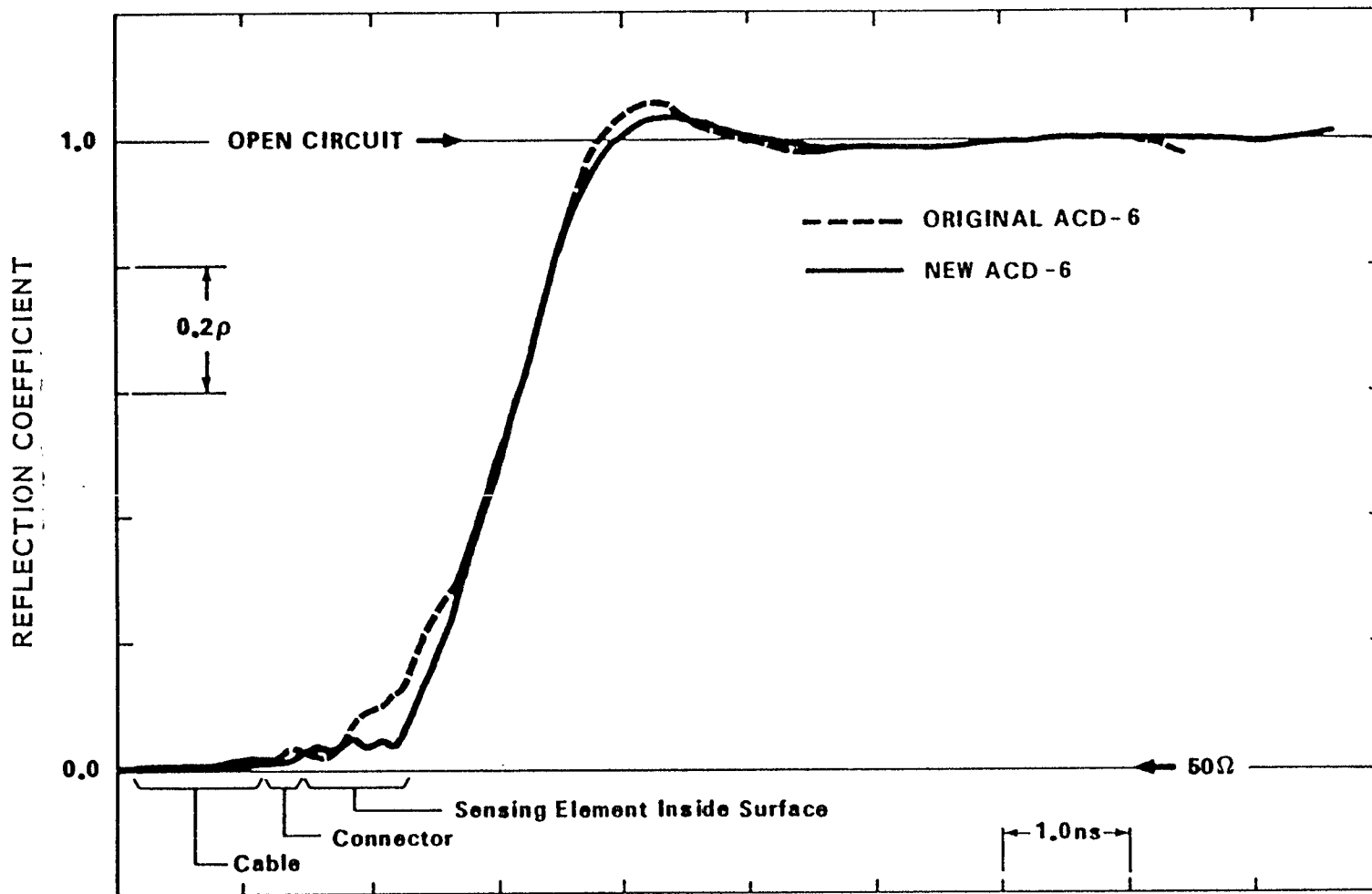


Figure 32. Old and New ACD-6 TDR Signatures

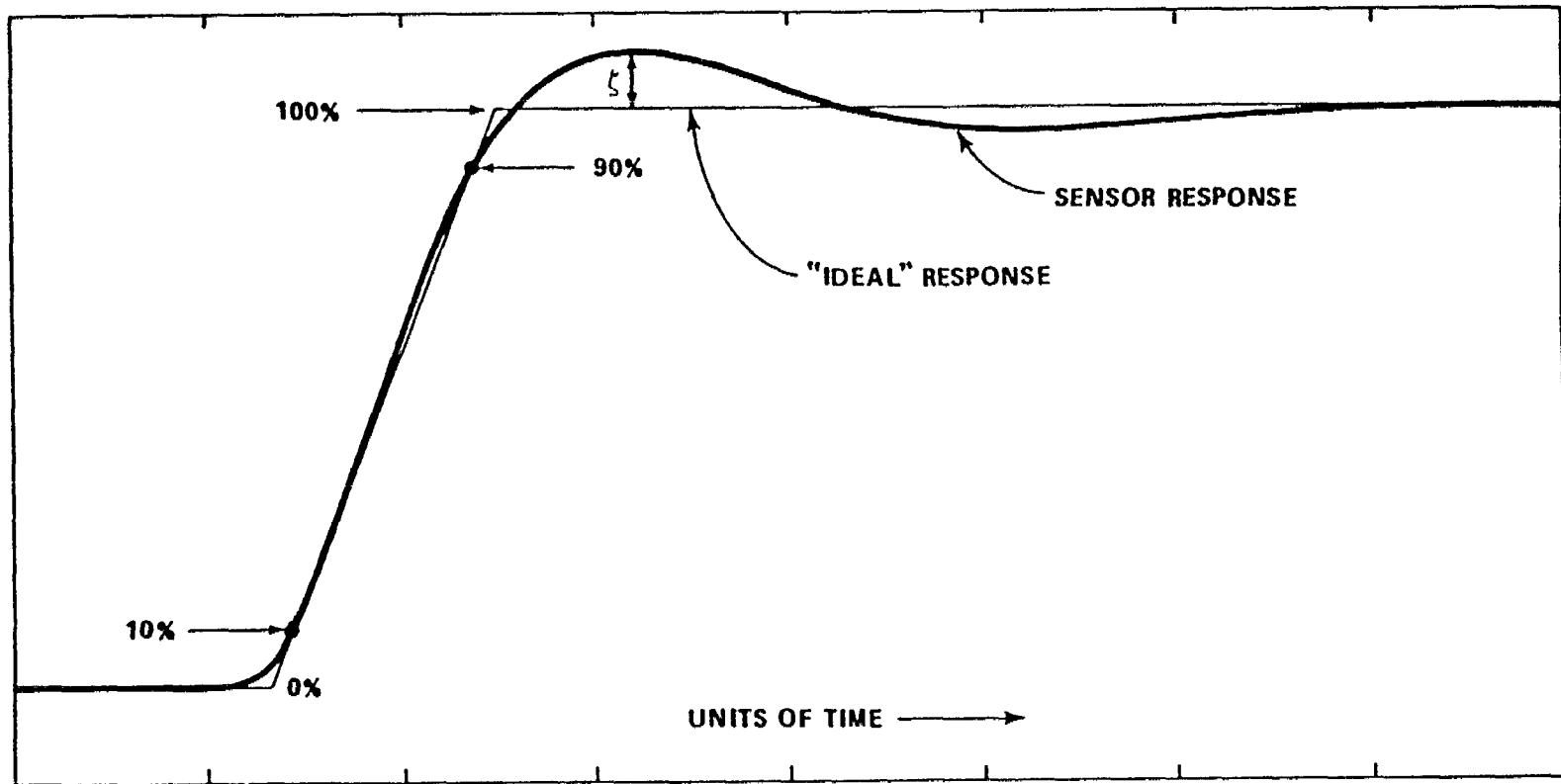


Figure 33. Pulse Fidelity Definition

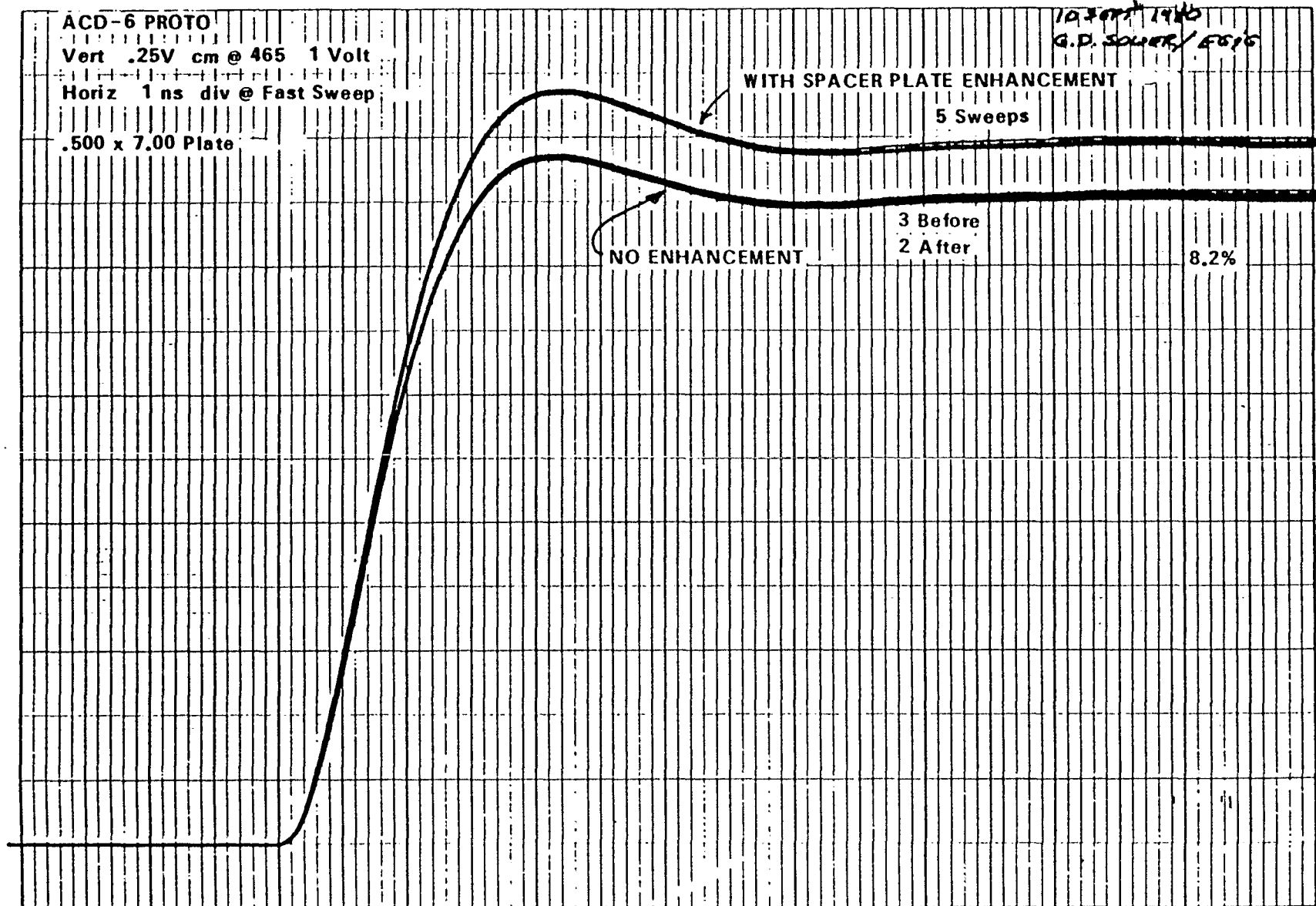


Figure 34. Enhancement Factor Data Measurement

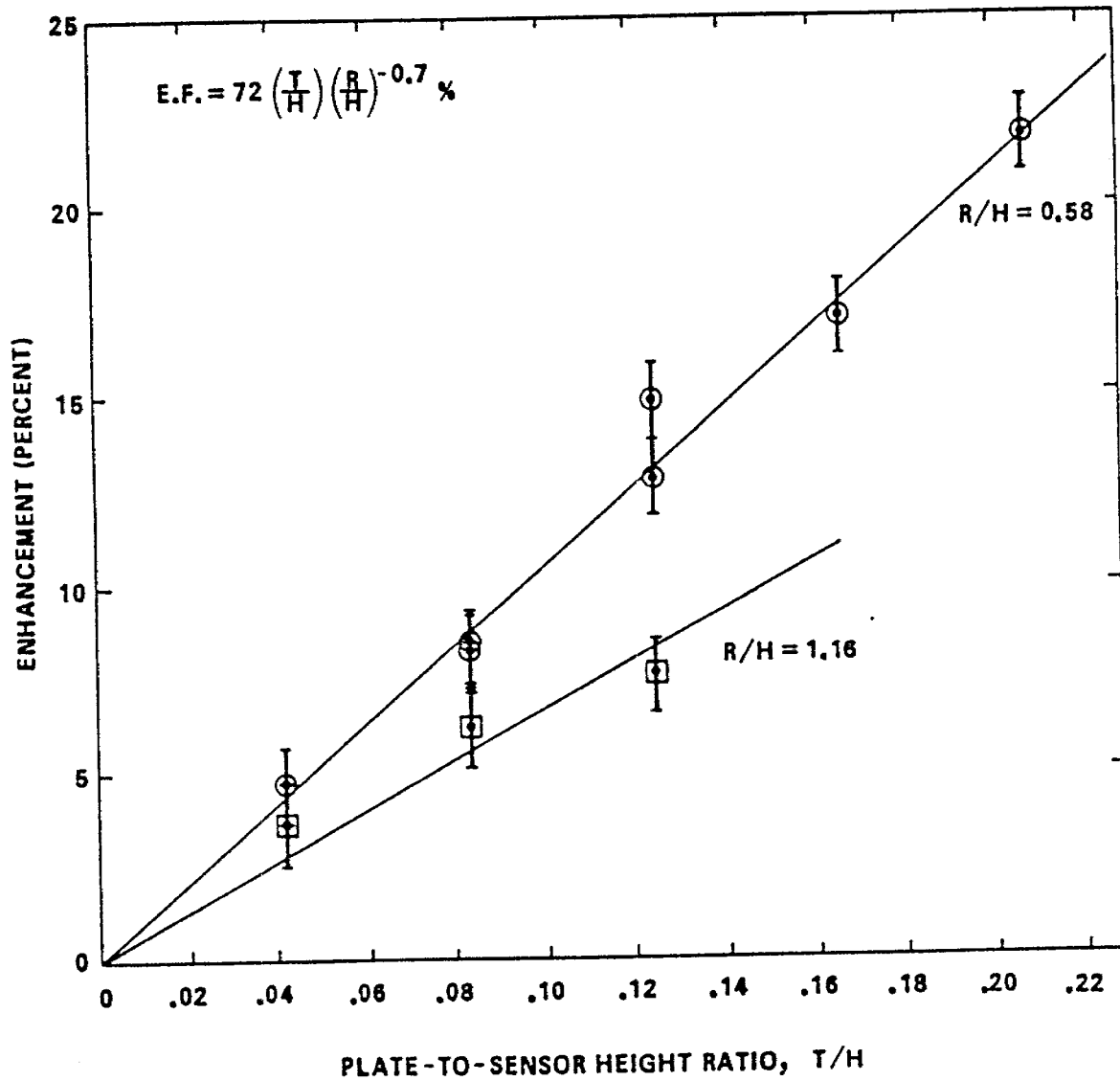


Figure 35. Enhancement Factor Data

APPENDIX A
DATA MEASUREMENT SYSTEM

The measurement system used to make measurements on the ACD sensors is shown in Figure A-1. The electromagnetic fields are generated on a Conical Elliptical Simulator. This consists of an elliptical ground plane with the drive cone apex at one focus and the sensor port at the other focus. The semi-major axis is 6.00 feet and the distance between the foci is 4.00 feet. It thus takes 4 ns for the signal from the cone to reach the sensor port while the first reflection from the simulator edge takes 12 ns. The simulator thus has 8 ns of clear time before any reflections reach the sensor.

The cone forms a 180-ohm transmission line above the ground plane. It is charged to some potential, nominally a few hundred volts, and then shorted to the ground plane at its apex through a very fast, mercury-wetted switch. This generates a step waveform which propagates spherically outward from the apex with an electric field given by

$$E_{\theta} = \frac{V_0}{r} \frac{60}{Z_c \sin \theta} \quad (\text{A-1})$$

where V_0 is the charge voltage, r is the radial distance from the apex, Z_c is the simulator characteristic impedance (180 ohms) and θ is the spherical coordinate measured from the center line of the cone. The cone is discharged to ground about 400 times per second so that repetitive pulse signals are measured by the sensor.

A screen room is located behind the ground plane of the simulator. The signal from the sensor is carried over high quality, solid jacket coaxial cable and enters the screen room via a bulkhead coaxial feedthrough. It is fed into the sampling oscilloscope at as high a level as can be obtained without saturating the sampling scope. A delay line is necessary in the present setup so as to delay the signal with respect to a trigger signal so that it can be displayed: A Tektronix 7M11 delay line is used, inserted in one of the slots in a Tektronix 7904 mainframe which is used for the oscilloscope. The 7M11 provides the needed 75 ns delay time, but has the undesirable property of adding a 175 ps rise time to the sensor data. From the 7M11, the

CONICAL ELLIPTICAL SIMULATOR

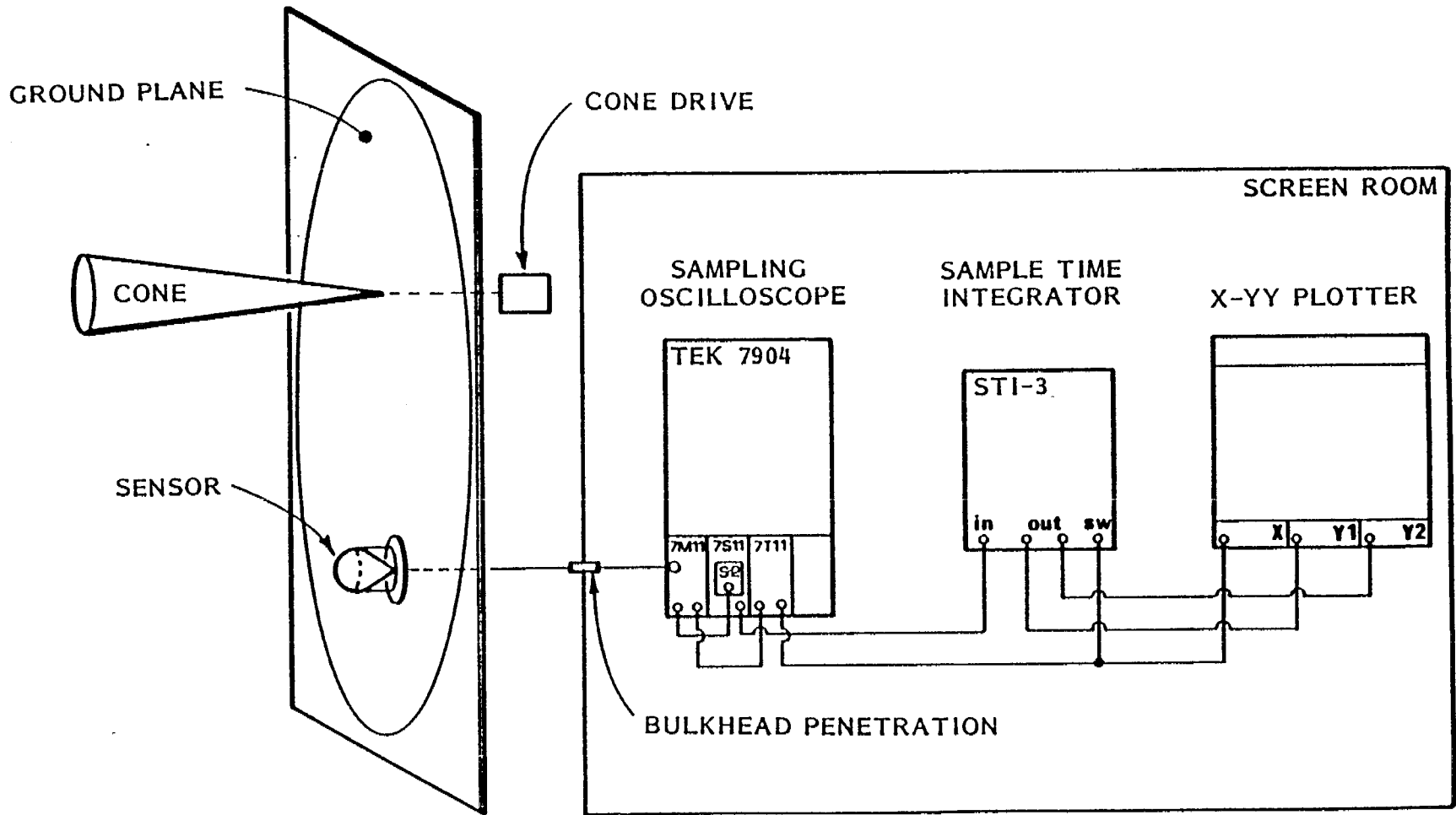


Figure A-1. Measurement System

signal, now attenuated by a factor of two, goes to the S-2 sampling head in the 7S11 sampling unit, which generates the sampling display. The S-2 has a rise time of 75 ps which, taken in quadrature with 175 ps from the 7M11, gives a rise time of 190 ps.

The sampling oscilloscope sweep is driven by a 7T11 time base, which is triggered by an external signal from a trigger probe near the cone on the simulator. The actual time base is generated by a very slow ramp external to the 7T11.

The external sweep is generated in the EG&G STI-3 Sample Time Integrator. This unit also takes the vertical output of the 7S11 and generates the two signals for the X-YY plotter. One of these signals is just the 7S11 output, buffered and amplified to drive the plotter. The other signal is the time-integral of the 7S11 output. This integration is performed in the slow sample-time of the sampling oscilloscope output, hence the name of the unit.

Errors in the integration of the sensor data occur because of noise generated by the sampling process. The noise output of the sampling oscilloscope is a constant level, so the signal input and output of the 7S11 are made as large as possible to maximize the signal-to-noise ratio. Special procedures are used in the STI-3 to minimize the effects of the residual noise, but it still creates about a one percent error in the final position of the integrated data trace.